An Integrated Multiscale Method for the Characterisation of Active Faults in Offshore Areas. The Case of Sant'Eufemia Gulf (Offshore Calabria, Italy)

Corradino, M.; Pepe, F.; Burrato, P.; Kanari, M.; Parrino, N.; Bertotti, G.; Bosman, A.; Casalbore, D.; Ferranti, L.; More Authors

DOI
10.3389/feart.2021.670557

Publication date
2021

Document Version
Final published version

Published in
Frontiers in earth science

frontiers in Earth Science

ORIGINAL RESEARCH
published: 11 June 2021
doi: 10.3389/feart.2021.670557

An Integrated Multiscale Method for the Characterisation of Active Faults in Offshore Areas. The Case of Sant'Eufemia Gulf (Offshore Calabria, Italy)

M. Corradino[1,2], F. Pepe[1], P. Burrato[3], M. Kanari[4], N. Parrino[1], G. Bertotti[5], A. Bosman[6], D. Casalbore[7], L. Ferranti[3,8,9], E. Martorelli[6], C. Monaco[2,9,10], M. Sacchi[11] and G. Tibor[4]*

[1]Dipartimento di Scienze della Terra e del Mare, Università di Palermo, Palermo, Italy, [2]Dipartimento di Scienze Biologiche, Geologiche ed Ambientali, Università di Catania, Catania, Italy, [3]Istituto Nazionale di Geofisica e Vulcanologia, Roma, Italy, [4]Department of Marine Geology and Geophysics, Israel Oceanographic and Limnological Research, Haifa, Israel, [5]Department of Civil Engineering and Geosciences, Delft University of Technology, Delft, Netherlands, [6]Istituto di Geologia Ambientale e Geoingegneria, Consiglio Nazionale delle Ricerche (IGAG-CNR), Roma, Italy, [7]Dipartimento Scienze della Terra, Sapienza Università di Roma, Roma, Italy, [8]Dipartimento di Scienze della Terra, dell'Ambiente e delle Risorse, Università di Napoli "Federico II", Napoli, Italy, [9]CRUST-DiSTAR, Centro inter Universitario per L'analisi SismoTettonica Tridimensionale con Applicazioni Territoriali, Università G. d'Annunzio, Chieti Scalo, Italy, [10]Istituto Nazionale di Geofisica e Vulcanologia, Osservatorio Etneo, Catania, Italy, [11]Consiglio Nazionale delle Ricerche - Istituto di Scienze Marine, Sede Secondaria di Napoli, Napoli, Italy*

OPEN ACCESS

Edited by:
Paola Vannucchi,
University of Florence, Italy

Reviewed by:
Sabina Bigi,
Sapienza University of Rome, Italy
Andrea Zanchi,
University of Milano-Bicocca, Italy
Derek Keir,
University of Southampton, United Kingdom

***Correspondence:**
F. Pepe
fabrizio.pepe@unipa.it

Specialty section:
This article was submitted to Structural Geology and Tectonics, a section of the journal Frontiers in Earth Science

Received: *21 February 2021*
Accepted: *31 May 2021*
Published: *11 June 2021*

Citation:
Corradino M, Pepe F, Burrato P, Kanari M, Parrino N, Bertotti G, Bosman A, Casalbore D, Ferranti L, Martorelli E, Monaco C, Sacchi M and Tibor G (2021) An Integrated Multiscale Method for the Characterisation of Active Faults in Offshore Areas. The Case of Sant'Eufemia Gulf (Offshore Calabria, Italy). Front. Earth Sci. 9:670557. doi: 10.3389/feart.2021.670557

Diagnostic morphological features (e.g., rectilinear seafloor scarps) and lateral offsets of the Upper Quaternary deposits are used to infer active faults in offshore areas. Although they deform a significant seafloor region, the active faults are not necessarily capable of producing large earthquakes as they correspond to shallow structures formed in response to local stresses. We present a multiscale approach to reconstruct the structural pattern in offshore areas and distinguish between shallow, non-seismogenic, active faults, and deep blind faults, potentially associated with large seismic moment release. The approach is based on the interpretation of marine seismic reflection data and quantitative morphometric analysis of multibeam bathymetry, and tested on the Sant'Eufemia Gulf (southeastern Tyrrhenian Sea). Data highlights the occurrence of three major tectonic events since the Late Miocene. The first extensional or transtensional phase occurred during the Late Miocene. Since the Early Pliocene, a right-lateral transpressional tectonic event caused the positive inversion of deep (>3 km) tectonic features, and the formation of NE-SW faults in the central sector of the gulf. Also, NNE-SSW to NE-SW trending anticlines (e.g., Maida Ridge) developed in the eastern part of the area. Since the Early Pleistocene (Calabrian), shallow (<1.5 km) NNE-SSW oriented structures formed in a left-lateral transtensional regime. The new results integrated with previous literature indicates that the Late Miocene to Recent transpressional/transtensional structures developed in an ~E-W oriented main displacement zone that extends from the Sant'Eufemia Gulf to the Squillace Basin (Ionian offshore), and likely represents the upper plate response to a tear fault of the lower plate. The quantitative morphometric analysis of the study area and the bathymetric analysis of the Angitola Canyon indicate that NNE-SSW to NE-SW trending anticlines were negatively reactivated during the last tectonic phase. We also suggest that

the deep structure below the Maida Ridge may correspond to the seismogenic source of the large magnitude earthquake that struck the western Calabrian region in 1905. The multiscale approach contributes to understanding the tectonic imprint of active faults from different hierarchical orders and the geometry of seismogenic faults developed in a lithospheric strike-slip zone orthogonal to the Calabrian Arc.

Keywords: active tectonics, calabrian arc (Italy), southern tyrrhenian sea, slab-tear fault, high-resolution seismic data, morphotectonic analysis

INTRODUCTION

Identifying seafloor scarps in bathymetry and the offset of Middle to Upper Quaternary marine deposits in seismic images are typically used in offshore areas to infer active faults and derive their geometric and kinematic characteristics that are necessary to parametrise seismogenic sources. Among the geophysical methodologies used to detect active faults, the high-resolution seismic reflection imaging provides a powerful tool to unravel the Late Quaternary activity of faults, to measure the displacements along the fault planes and to correlate the onshore with the offshore segments (e.g., Barreca et al., 2014; Barreca et al., 2018; Ferranti et al., 2014; Cultrera et al., 2017a; Corradino et al., 2021). Standard methods for qualitative morphotectonic analysis that use multibeam high-resolution bathymetric data consist of tracing in plan-view the faults that offset the seafloor and in recognising morphological features close to the tectonic structures, such as rectilinear canyons, scarps or seafloor undulations (e.g., Fracassi et al., 2008; Di Bucci et al., 2009; Loreto et al., 2013; Cultrera et al., 2017b; Loreto et al., 2021). However, a limitation in reconstructing complex structural pattern in offshore areas is caused by the difficulty in mapping faults in areas not fully covered by geophysical data, by the low preservation potential of fault scarps and, often, by the blind nature of the tectonic deformation occurring when the structures do not produce detectable deformation at shallow depth (due to their geometry and depth). Consequently, an approach that includes only observation of the seafloor and superficial deposits can be insufficient and misleading for identifying the primary active faults associated with the most significant seismic moment release. Most shallow faults may be secondary features formed in response to local stresses (e.g., bending moment normal faults that occur on the top of a reverse structure) and are not the direct surface expressions of primary structures. Besides, the primary active faults can exploit inherited faults in response to a change of the regional stress regime, further complicating the interpretation. The question tackled in this work is what is the correct approach in the offshore area to identify and characterise primary active faults that can be potentially seismogenic?.

We test a multiscale and multidisciplinary approach to detect surficial and blind active faults, and distinguish the tectonic imprint of active faults from different hierarchical orders. Our method is based on the integration of seismic reflection data with different resolution/penetration and the quantitative morphometric analysis of a high-resolution multibeam bathymetric dataset. The approach significantly differs from the standard because the quantitative analysis of the bathymetry can identify seafloor areas in a transient state caused by fault-related deformation, even if these areas are not fully covered by seismic reflection data.

The site chosen for testing the method is the Sant'Eufemia Gulf (Tyrrhenian offshore the central Calabrian Arc, **Figures 1A,B**) because it can be considered as a natural laboratory to investigate the complex relationships between regional and local processes due to the presence of a slab tear in the Calabrian subduction system (Rosenbaum et al., 2008; Neri et al., 2009; Maesano et al., 2017; Scarfì et al., 2018) and, at shallower levels, of crustal faults that controlled the Plio-Quaternary tectonic evolution (Del Ben et al., 2008; Loreto et al., 2013; Brutto et al., 2016). This region was also the epicentral area of the Mw 7.0, 1905 central Calabria destructive earthquake (Rovida et al., 2020). The seismogenic source of this event is still poorly constrained and debated (DISS Working Group, 2018) due to its offshore location and the limited seismic instrumental records.

GEOLOGICAL SETTING

SE Tyrrhenian Basin and the Adjacent Calabrian Arc

The Tyrrhenian basin developed since Late Miocene within the frame of Europe-Africa convergence and was mainly controlled by the westward and northwestward subduction of the Adriatic and Ionian lithosphere (Carminati et al., 1998; Faccenna et al., 2001; Carminati and Doglioni, 2005). The upper plate of the subduction system, from west to east, consists of back-arc basins that appear younger southeastwards (Vavilov and Marsili basins; Carminati and Doglioni, 2005; Faccenna et al., 2001; Faccenna et al., 2007), an arc-shaped volcanic ridge (i.e., Aeolian islands), and a forearc region including the Calabrian Arc and the Calabrian accretionary wedge (Corradino et al., 2020; Pepe et al., 2010; **Figures 1A,B**).

The subducting lithosphere dips ~70–80° northwestward (Wortel and Spakman, 2000; Piromallo and Morelli, 2003; Chiarabba et al., 2008; Scarfì et al., 2018). Seismic tomography data highlights positive P wave anomalies (Lucente et al., 1999) in the subducting lithosphere, interpreted as the signature of slab breakoff beneath the northern Calabrian Arc (Neri et al., 2009; Maesano et al., 2017; Scarfì et al., 2018; **Figure 1C**), and sub-vertical tears in the slab that propagates perpendicular to its strike (Rosenbaum et al., 2008, **Figure 1D**). Tearing and segmentation of subducting oceanic lithosphere are common processes in subduction systems (Chatelain et al., 1992; Carminati et al.,

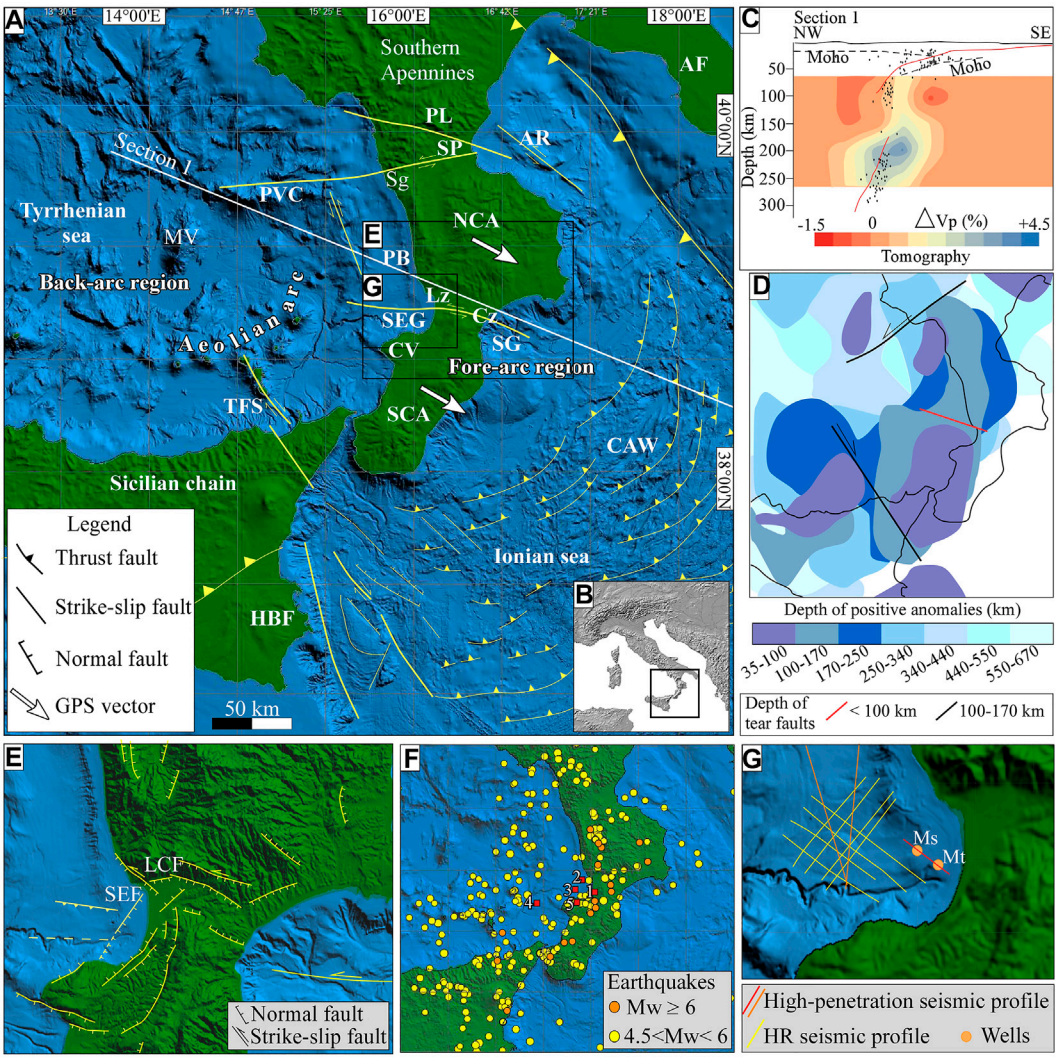

FIGURE 1 | (A) Schematic tectonic map of the Tyrrhenian-Ionian subduction system. AF, Apulian foreland; AR, Amendolara ridge; CAW, Calabrian accretionary wedge; CV, Capo Vaticano; Cz, Cosenza; HBF. Hyblean foreland; Lz, Lamezia; MV, Marsili volcano; NCA, northern Calabrian Arc; PB, Paola basin; PL, Pollino; PVC, Palinuro volcano complex; SCA, southern Calabrian Arc; SEG, Sant'Eufemia Gulf; Sg, Sangineto; SG, Squillace Gulf, SP, Sibari Plain; TFS, Tindari fault system. **(B)** Location of the area shown in panel a. **(C)** Section across the slab (modified from Maesano et al., 2017). Redline is the position of the subduction interface. Black dots are the earthquakes collected in 10-km wide buffers around the section trace. The dashed black line is the position of the Moho from Scrocca et al., 2003. Tomographic data are from Neri et al., 2009. **(D)** Upper mantle structure based on positive P wave seismic anomalies (modified from Rosenbaum et al., 2008). The coloured areas represent positive anomalies at different depth ranges. Rosenbaum et al., 2008 interpreted these areas as remnant subducting slabs, separated by tear faults (black and red lines). **(E)** Schematic tectonic map of the central Calabrian Arc (modified from Monaco and Tortorici, 2000; Brutto et al., 2016) and offshore (modified from Loreto et al., 2013; Del Ben et al., 2008). LCF, Lamezia-Catanzaro Fault; SEF, Sant'Eufemia Fault. **(F)** Distribution of instrumental earthquakes recorded since 1985 up-to-date, from INGV Seismic Bulletin (ISIDe Working Group, 2007; http://iside.rm.ingv.it). Red squares indicate the 1905 epicentral location proposed by (1) Rizzo, (1906), (2) Riuscetti and Schick, (1975), (3) Camassi et al. (1997), (4) Michelini et al. (2006), (5) Guidoboni et al. (2007). **(G)** Grid of high-penetration and high-resolution (HR) seismic profiles used for this study. Ms, Marisa well; Mr, Marta well.

1998; Wortel and Spakman, 2000; Lallemand et al., 2001; Levin et al., 2002; Miller et al., 2006). These processes can be consequent to 1) changes in the velocity of subduction rollback (Govers and Wortel, 2005), 2) the lateral variation of nature (continental or oceanic) or thickness of the slab (Argnani, 2009), 3) local collisional events (Sacks and Secor, 1990). E-W trending deep tear faults (greater than 340 km) were detected in the northern Tyrrhenian sea. These tear faults continue at slightly shallower depths (<340 km) beneath the north and central Apennines with a NNE-SSW orientation (see Figure 5 in Rosenbaum et al., 2008). Shallower (between 100 and 340 km) NE-SW and NW-SE trending tear faults were interpreted beneath the southern Apennines and eastern Sicily, respectively (**Figure 1D**). These tear faults accommodate vertical or oblique to horizontal motion (or both) between the two blocks of the subducting slab across their strike and dip-to strike-slip movements in the upper plate (Govers and Wortel, 2005; Rosenbaum et al., 2008; Baes et al., 2011). At the edges of the subducting lithosphere, Subduction-

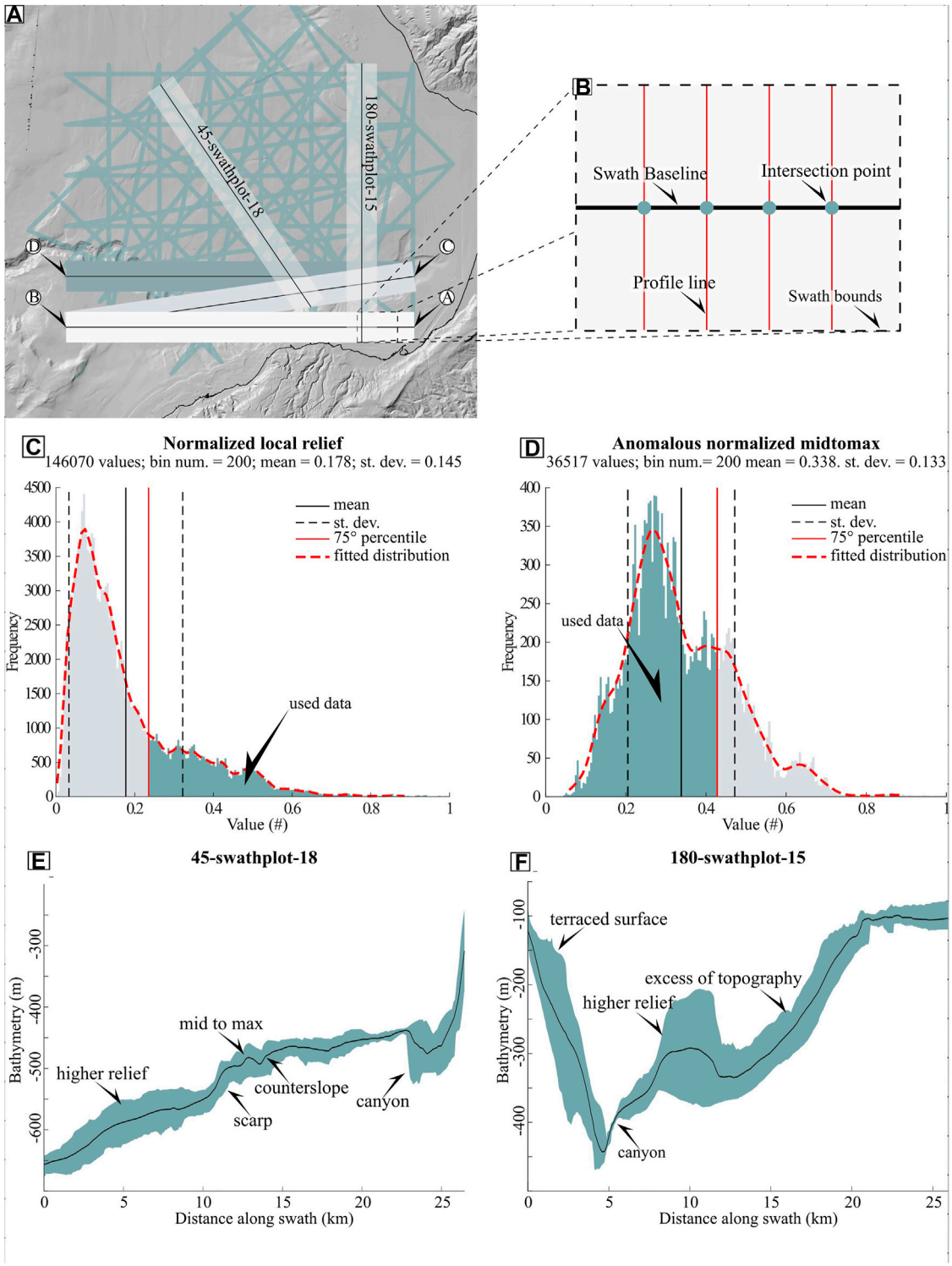

FIGURE 2 | A) Map view of the swath profile grid used for the seafloor morphometric analyses. The two swath profiles labelled "45-swathplot-18" and "180-swathplot-15", shown in **(C and D)**, respectively, are highlighted with the white transparent band. Capital letters, from A to D, into white circles, represent the edges of the swath profile segments in white, light grey, and light green. **(B)** Conceptual sketch representing the zoom of the initial portion of the white swath profile of the previous inset. The thick black line represents the swath profile baseline, the dashed black line represents the swath profile bounds, and the thin red lines represent the topographic profile lines. The light green circles represent the intersection points between the profile lines and baseline. **(C)** Frequency histogram of the normalised local relief data distribution. Values higher than the 75% percentile, in light green, represent the highest computed local relief values. **(D)** Frequency histogram of the anomalous normalised mid-to-max data distribution. Values lower than the 75% percentile relate to areas where the mean bathymetry significantly approaches higher bathymetry values. **(E)** Swath profile labelled 45-swathplot-18 highlighting the presence of a scarp and a counter-slope area in the Gulf central sector. **(F)** Swath profile labelled 180-swathplot-15 evidencing a significantly higher relief detected in correspondence of a bathymetric ridge.

Transform Edge Propagator (STEP, also called tear) faults occur (Gallais et al., 2013; Orecchio et al., 2014; Gutscher et al., 2016; Maesano et al., 2020). STEP faults produce tearing in the slab and generally propagate perpendicular to the subduction strike (Nijholt and Govers, 2015). Most of them show vertical motion between the two blocks of the underthrusting plate at both sides of the STEP fault and normal to strike-slip movements in the upper plate (Govers and Wortel, 2005; Baes et al., 2011).

The Calabrian Arc is an allochthonous block of continental crust (Calabria–Peloritani terrane after Bonardi et al., 2001) that connects the southern Apennines with the Sicilian-Maghrebides chain (**Figure 1A**). Its arcuate shape can be attributed to the Apennine belt's diachronous collision with the Apulian foreland to the north and with the Hyblean foreland to the south (Malinverno and Ryan, 1986; van Dijk et al., 2000). Strike-slip fault systems developed both oblique and perpendicular to the orogenic belt. These fault zones caused the fragmentation of the Calabrian Arc in NW-SE elongated blocks that have moved independently southeastwards with different displacements and rotations (Knott and Turco, 1991; van Dijk and Okkes, 1991; van Dijk, 1992; van Dijk and Scheepers, 1995). The major strike-slip fault systems are the Pollino and Sangineto system to the north and their offshore prolongations (Ferranti et al., 2009; Ferranti et al., 2014; De Ritis et al., 2019), the Lamezia-Catanzaro line in the central sector (Neri et al., 1996; Tansi et al., 2007; Del Ben et al., 2008), and the Tindari line in the north-eastern Sicily (**Figure 1A**; Billi et al., 2006; Cultrera et al., 2017b). Both the northern and the southern strike-slip zones represent the upper plate expression of the Ionian slab STEP faults (Doglioni et al., 2001; Govers and Wortel, 2005; Rosenbaum et al., 2008; Polonia et al., 2016; De Ritis et al., 2019; Maesano et al., 2020; **Figures 1A,D**).

NNW-SSE strike-slip fault systems also affected both the Tyrrhenian and Ionian offshore of the northern Calabrian Arc (i.e., Paola Basin in the Tyrrhenian offshore, and the Amendolara Ridge in the Ionian offshore, PB and AR in **Figure 1A**) during the Late Pliocene—Early Pleistocene (Ferranti et al., 2014; Corradino et al., 2020).

The Lamezia-Catanzaro System and Surroundings Offshore Areas

The Lamezia-Catanzaro system is a WNW-ESE trending strike-slip fault system (**Figures 1A,E**) that separates the northern and southern parts of the Calabrian Arc (van Dijk et al., 2000; Tansi et al., 2007). In the western offshore of the Catanzaro trough (Sant'Eufemia Gulf in **Figure 1A**), Loreto et al. (2013) recognise three main tectonic features affecting the Plio-Quaternary basin infill. These structures are 1) a ~13 km long, N31° striking normal fault that offsets seismic reflectors up to the seafloor (SEF in **Figures 1E**, **2**) a WNW-striking polyphase fault system, and 3) a likely E-W trending lineament (**Figure 1E**). Two deep wells were drilled in the Sant'Eufemia Gulf (Marisa and Marta, Mr and Mt in **Figure 1G**). The stratigraphic succession indicates a metamorphic basement covered by Messinian deposits, overlain by Pliocene fine-grained deposits (mudstone and claystone), and Pleistocene coarser deposits (sandstone and siltstone).

Brutto et al. (2016) based on structural data acquired in the western Catanzaro basin and its offshore prolongation in the Sant'Eufemia Gulf, document 1) a left lateral NW-SE oriented fault system that affects upper Miocene deposits, 2) right-lateral NE-SW oriented faults that involve Piacenzian-Lower Pleistocene units and led to the development of structural highs in the eastern sector of the gulf and 3) NE-SW and, subordinately, N-S oriented normal faults that affect Middle Pleistocene to Recent deposits.

Based on the analysis of the depth variation of the edges of Infralittoral Prograding Wedges, Pepe et al. (2014) documented difference in the post-Last Glacial Maximum vertical tectonic movements between the SW and NE offshore sectors of the Capo Vaticano promontory (western Calabria, southern Italy). Offshore of Capo Vaticano promontory, Pleistocene intrusive, and off-arc volcanic activities occurred (De Ritis et al., 2010; Loreto et al., 2015). The uprising of magma was favoured by Pliocene NW- and Pleistocene NE-trending normal fault systems.

The eastward offshore prolongation of the Lamezia-Catanzaro line lies in the Squillace Gulf (**Figures 1A,E**). Here, a W-E trending, transtensional basin developed during the Pliocene (Del Ben et al., 2008).

Seismotectonic Framework

The western margin of the central Calabrian Arc is an area of large seismic moment release (**Figure 1F**; CFTI5Med, Guidoboni et al., 2018; CPTI15, Rovida et al., 2020; Rovida et al., 2021), where destructive historical earthquakes have been generated by onland crustal seismogenic sources (Tiberti et al., 2017; DISS Working Group, 2018). The seismogenic activity of the Ionian subducting lithosphere is highlighted by the deep seismicity down to ~600 km beneath the Tyrrhenian Sea (Chiarabba and Palano, 2017). Despite the evidence of seismogenic activity, no large inter-plate historical or instrumental earthquakes have been documented so far, being the deep seismicity interpreted as intraslab events (**Figure 1C**; Chiarabba et al., 2015). Only the 1905 earthquake has been tentatively interpreted by some authors as a plate interface event (e.g., Galli and Molin, 2009; Presti et al., 2017). However, this earthquake is still poorly documented, and it has uncertain magnitude estimates and epicentral locations, most of them offshore (**Figure 1F**, see Sandron et al., 2015 for a review of the studies on the 1905 earthquake). Nonetheless, modelling of GPS velocities shows that the subduction may be locked and capable of large magnitude earthquakes with long return times (Carafa et al., 2018).

The INGV instrumental catalogue shows that the largest seismic events in the past 35 years have epicentres located in the Tyrrhenian offshore and hypocentre deeper than 100 km (maximum Mw 5.8, October 26, 2006 earthquake at 221 km of depth; ISIDe Working Group, 2007). Conversely, the onland seismicity is located up to 20 km depth (maximum Mw 3.9). Only shallow, scattered events were localised in the Ionian offshore.

The historical seismicity indicates that the Calabrian Arc is one of the most seismic areas of the whole Italian territory. The area between the Messina Straits and the Catanzaro trough was affected by several large earthquakes (Mw > 6), among these, the 1,783 seismic events (February 5, Mw 7.1, February 7, Mw 6.7,

and March 28, Mw 7.0), 1905 (Mw 7.0) and 1908 (Mw 7.1) events, which were generated by crustal faults (DISS Working Group, 2018).

Active deformation data (GPS, Devoti et al., 2017; focal mechanisms, Totaro et al., 2016, Pondrelli et al., 2020; active stress indicators, IPSI database, Mariucci and Montone, 2020) show that the central sector of the Calabrian Arc is characterised by an NW-SE oriented extensional tectonic regime, responsible for large magnitude earthquakes (e.g., Galli and Peronace, 2015). Towards the east, the Ionian offshore area undergoes a transcurrent regime due to the oblique plate convergence (Totaro et al., 2016), and is affected by active compressional structures related to the Calabrian subduction complex (e.g., Polonia et al., 2011; Gutscher et al., 2017).

The seismotectonic interpretation of the seismicity may be broadly divided into two alternative models (see Tiberti et al., 2017 for a review). The first model, described as the "Siculo-Calabrian Rift Zone" (Tortorici et al., 1995; Monaco and Tortorici, 2000), considers a system of W-dipping high-angle surface normal faults as the source of the largest earthquakes. The second one, named as "Subduction-top model" (Tiberti et al., 2017) and implemented in the DISS database (DISS Working Group, 2018), highlights the role of east-dipping, low angle, blind normal faults, antithetic to the subduction system, located along the Tyrrhenian side of the Calabrian Arc. In the latter model, the longitudinal normal fault systems are dissected by strike-slip faults zone crossing the Calabria Arc. The transversal faults have deemed the sources of earthquakes occurring at the edges of the longitudinal seismogenic segments. The W-dipping faults are considered shallow antithetic faults respect to the E-dipping ones, as shown, for example, in the Messina Straits area (Bonini et al., 2011).

DATA AND METHODS

Multibeam Bathymetry

The high-resolution Digital Elevation Model (DEM) is a part of the multibeam bathymetric dataset acquired and processed by the National Research Council (IGAG) between 2010 and 2013. Bathymetric data were collected using multibeam systems at different frequencies. In shallow water, the Kongsberg EM 3002D (300 kHz), EM 710 (10–100 kHz) and Reson SeaBat 7111 (100 kHz) systems were used, while in deep waters, Reson SeaBat 7160 (44 kHz) was used.

During the bathymetric surveys, multibeam transducers' calibration in areas close to the survey zone was performed together with sound velocity profiles. The Caris Hips and Sips hydrographic software processed all bathymetric datasets. Data processing included: 1) patch test on calibration lines, 2) tide corrections, 3) statistical and geometrical filters to remove coherent and incoherent noise, 4) manual removal of spikes.

Processed data were gridded, generating DEMs with cell size varying from 0.5–1 m in shallow water (<100 m) to 10 m in intermediate water (100–500 m) and 15–20 m in deep water (>500 m). In this work, the DEM was at 15 m gridded resolution, and the bathy-morphological map was projected in UTM 33N—Datum WGS84.

Seismic Reflection Data Acquisition and Processing

Over 500 km of multichannel high-penetration reflection seismic data (Airgun) and high-resolution (HR) multichannel seismic reflection data (Geo-Source Sparker) were recorded in the Sant'Eufemia Gulf in 1999 and 2019, respectively (orange and yellow lines in **Figure 1G**). Airgun profiles are oriented from NNW–SSE to NNE–SSW directions. Geo-Source Sparker inline profiles are primarily oriented in the NW–SE to N–S directions, with crossline seismic profiles acquired along the NE–SW direction. A DGPS system controlled the navigation positioning for all datasets. This paper presents a subset of these data consisting of seismic lines oriented from NW-SE to NE-SW.

A high-resolution 48-channel seismic reflection system with slant streamers and group spacing varying from 1 to 2 m recorded the signals generated by an innovative multi-tip (400) Sparker array in a dual-source Sparker system based on negative discharge technology. The shooting interval was 2.0 s, with a 1.5 s record length and 0.1 ms sampling interval. An innovative differential GPS positioning system was used to perform all necessary computations to determine real-time positions of sources and receivers. The processing sequence included the following operations: geometry assignment by 2D CDP profiles binning, DC removal, signature deconvolution, F-K filter, trace stacking, static corrections, velocity analysis, multiple attenuation, post-stack Kirchhoff time migration, receiver deghosting, time-variant bandpass filtering and automatic gain control removal to restore the True Amplitude. Signal penetration exceeds 500 ms two-way time (t.w.t). Vertical resolution reached up to 0.25 m near the seafloor.

The Geo-Suite AllWorks software package was used to process single-channel reflection seismic data and for seismic interpretation. Seismo- and sequence stratigraphy based analysis facilitated the reconstruction of the depositional architecture of seismic-stratigraphic units.

An additional MCS profile from Vi.DE.PI database (red line in **Figure 1G**, https://www.videpi.com/videpi/sismica/sismica.asp) was used for this study. The MCS section was converted from raster to SEG-Y format using the GeoSuite AllWorks software. The geodetic reference system is the WGS84 with a UTM 33 N projection.

Morphotectonic Analysis

Two grids of 50 swath profiles covering roughly 1,000 km^2 were used to analyse the relief distribution and the topographic response to tectonic forcing (**Figure 2A**). Swath profiles sample topographic information from rectangular areas and include such information into an elevation profile by stacking multiple topographic profiles. The trace of these topographic profiles, here labelled as profile lines, are equally spaced and oriented perpendicularly to the swath profile baselines (**Figures 2A,B**). The same length characterises all the profile lines.

A 2 km swath width was adopted to highlight tectonic signals at the kilometric scale for detecting the primary faults in the study area. Two grids with N-S, E-W, NNW-ESE and ENE-WSW oriented segments define the baselines for the swath profiles (**Figure 2A**). The swath profiles were computed using a code wrapper employing the algorithms proposed by Schwanghart and Scherler, (2014). We extracted and listed endpoint coordinates of each grid segment, sampled two pairs of coordinates simultaneously, and computed the swath profiles between those extracted points. A grid of swath profiles oriented along with the directions of the segments above described, and the diagonal joining two adjacent segments was obtained (**Figure 2A**). For example, the first swath profile was created using the two coordinates labelled A and B, the second one using the coordinates B and C, and going in this way until using all the stored coordinates. The maximum, minimum, and mean values of bathymetric depth were sampled along each profile line (**Figure 2B**) and arranged as a matrix of 146,071 georeferenced points. The coordinates of each point correspond to the intersection between the profile lines and swath baselines (**Figure 2B**). The dataset was used to compute the local relief for each point as the difference between the maximum and minimum value sampled for each profile. This value corresponds to the local relief along the profile. Finally, the local relief was normalised dividing the data distribution by its maximum value, so the result values range from one to zero. Considering that values approaching one represents the maximum computed relief, the 75° percentile of this distribution was considered as the minimum threshold to detect the areas with the highest relief values (**Figure 2C**). The mean elevations approaching the maximum ones were detected within these areas to infer the bathymetric response to the tectonic forcing (Burbank and Anderson, 2011). To do this, we computed the mid-to-max value and filtered the dataset using the following equations:

$$\text{mid-to-max} = \max \text{bathymetry} - \min \text{bathymetry} \quad (1)$$

$$\text{anomalous} = (\max \text{bathymetry} - \min \text{bathymetry})/2 \quad (2)$$

The distribution of mid-to-max values ranging from one to zero was obtained by normalisation. The values approaching zero are areas controlled by the tectonic forcing. A threshold of values lower than the 75° percentile was applied to select the Anomalous Mid-To-Max (AMTM) values from this distribution. The resulting points (14,815) of AMTM values coincide in correspondence of high-relief areas where the submarine landscape responds to recent tectonic forcing (**Figure 2D**).

The bathymetric map and swath profiles were qualitatively analysed to identify morphologic signature related to nearby tectonic structures (**Figure 2D**). In particular, the upstream portion of the Angitola Canyon was analysed through a ~22 km-long trunk longitudinal profile and 23 bathymetric cross profiles. Such profiles were placed along the canyon to capture changes in the canyon aspect ratio by computing the height to width ratio (H/W). Finally, the spatial correlation among slope changes of the trunk stream long profile, H/W values, and the geographic and stereological properties of the main geologic structures detected closely were analysed to infer the possible response of the Angitola Canyon to the tectonic forcing.

RESULTS

Morpho-Bathymetry Analysis

The multibeam bathymetry of the study area shows a 1–9 km wide continental shelf, with the edge located between 140 and 160 m water depth. The shelf edge is irregular in plan-view because of the alternation of erosive features (canyon heads, gullies and landslide scars in **Figure 3**), carving the shelf, and submarine ridges developed on the continental slope. One of the prominent ridges, hereafter named Maida Ridge, is located just to the north of the Angitola Canyon between 120 and 400 m water depth (**Figure 3**). The Maida Ridge is a NE-SW-trending morphological high over 12 km long, has an average width of ~4 km, and a morphological relief of ~150 m. Smaller ridge-like structures are also developed in the northern part of the study area, just below the shelf facing the Falerna Marina village. As a whole, the continental slope has a mean gradient of 3–4° and displays an overall uneven morphology both in its upper and lower part. Notably, the main morphology recognisable in the slope between 450 and 700 m water depth is a mounded relief located in the center of the study area (Mounded relief in **Figure 3**). This feature is about 11 × 8 km in size and has a morphological relief of about 20 m with respect to the surrounding seafloor; two shallow and narrow erosional channels laterally bound it. In particular, a set of SW-NE elongated scarps affects the morphological high and its surroundings; these scarps are 2–8 km long and 2–10 m high.

The Angitola Canyon is the main bathymetric feature of the Sant'Eufemia Gulf. Its head lies at a water depth of about 100 m, along the offshore prolongation of the Angitola River. The canyon pattern is roughly rectilinear from the canyon head to ~560 m water depth. Below this depth, the pattern abruptly becomes meandering. Such a meandering pattern extends down to a regional NE-SW-trending scarp, which crosses the canyon at roughly 900 m water depth. After that, the canyon resumes a sub-rectilinear pattern.

Seismo-Stratigraphic Characterisation and Interpretation

In the high-penetration seismic profiles, two seismo-stratigraphic units, labelled from bottom to top as MD and PQ (**Figures 4A**, **5A**,**B**), were defined by their bounding unconformities and described based on their architecture and seismic characters (e.g., amplitude, lateral continuity, and frequency of internal reflectors). Seismic profiles were calibrated using well-log data (Cosentino et al., 2017; Ms and Mt in **Figure 1G**).

Unit MD is characterised by relatively discontinuous, medium frequency, and medium-to high-amplitude reflectors. It is bounded upwards by a well-defined, high-amplitude unconformity (M horizon in **Figure 4A**), associated with the top of evaporites deposited during the late Messinian salinity crisis or to an erosional unconformity formed during the late Messinian sea-level fall (Malinverno et al., 1981, and references therein). We correlate unit MD with the Upper Miocene deposits based on the seismic signature and well log data (**Figure 5B**).

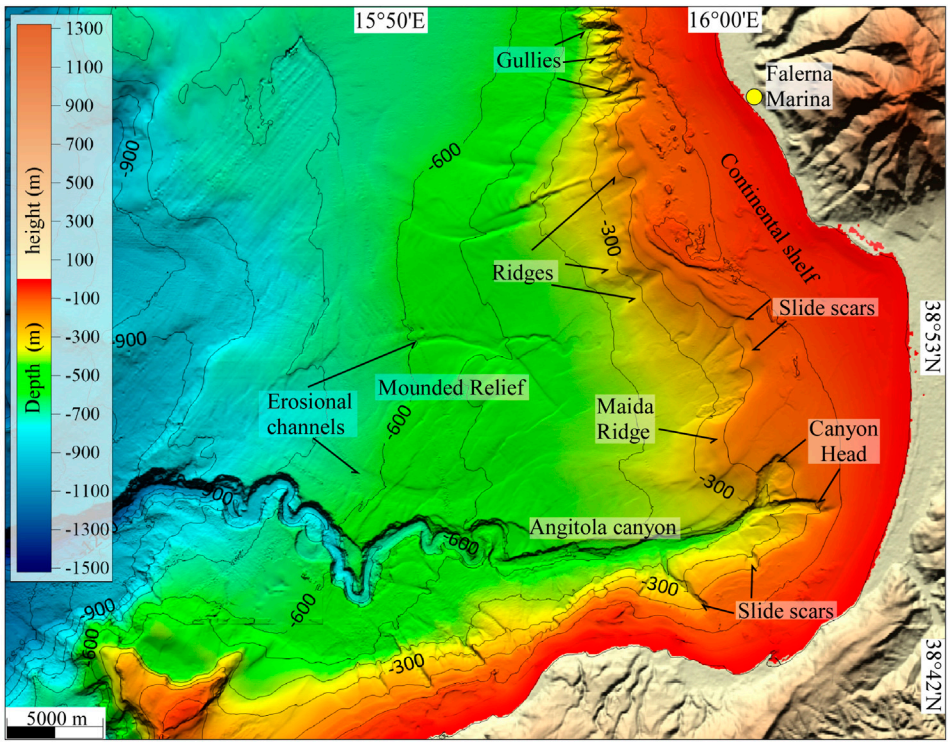

FIGURE 3 | Morphobathymetric map of the Sant'Eufemia Gulf.

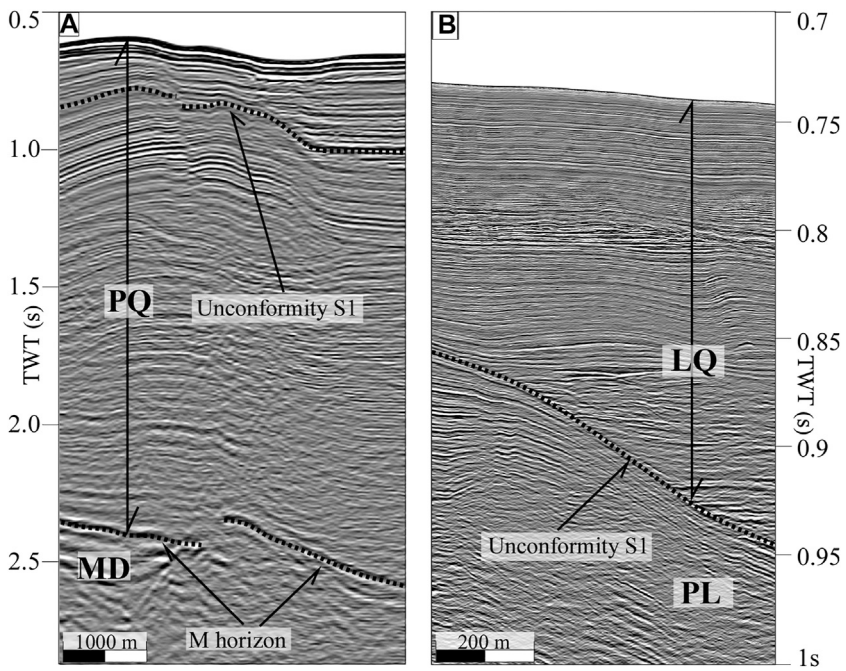

FIGURE 4 | (A) Seismostratigraphic units (MD and PQ) recognised on the high-penetration seismic profile "Line Sister—12". **(B)** Seismostratigraphic subunits (PL and LQ) recognised on the HR seismic profile "Line—04." See **Figure 5A** for location.

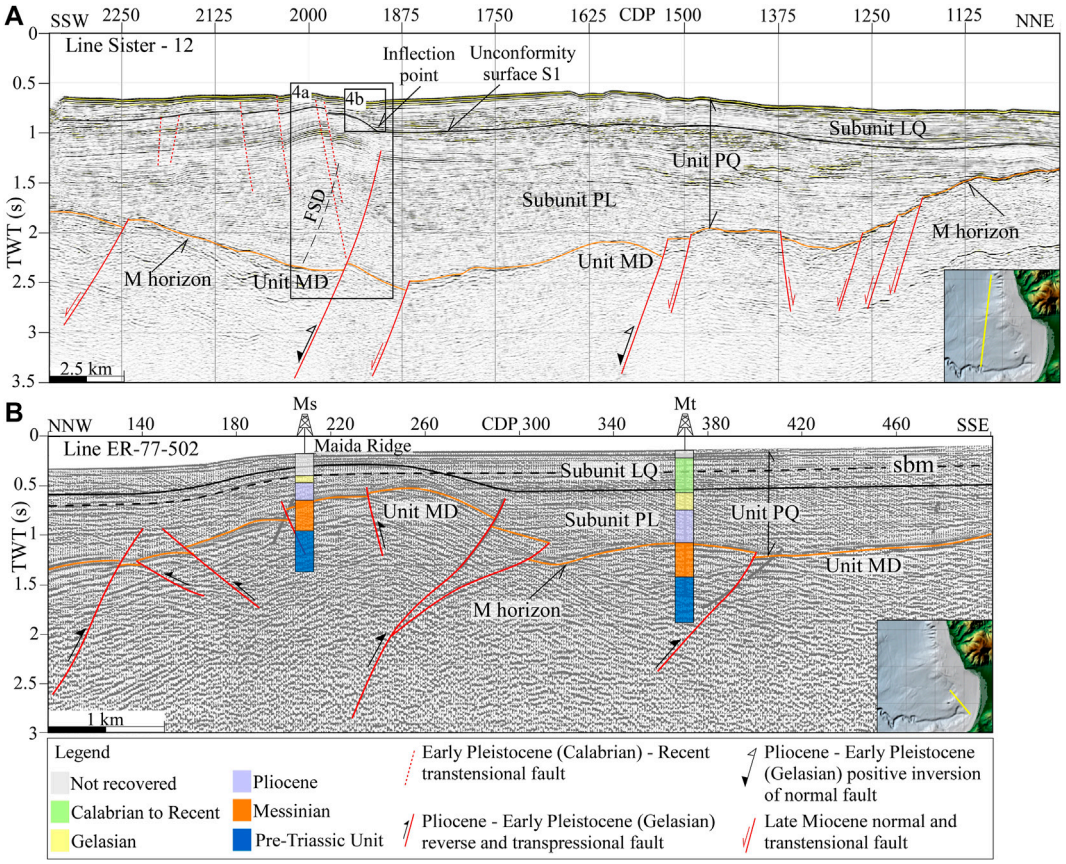

FIGURE 5 | (A) Seismic profile "Line Sister—12" and its interpretation. Boxes 4a and 4b are displayed in **Figure 4**. **(B)** Seismic profile "Line ER-77-502" and its interpretation. Insets show the location of the profiles. Ms, Marisa well; Mr, Marta well; FSD, fan-shaped deposits; sbm., seabed multiple; Unit MD, Upper Miocene deposits; Unit PQ, Plio Quaternary deposits; PL and LQ, subunits of the Plio Quaternary deposits.

Unit PQ overlays the M horizon and shows continuous, high- to medium-frequency and medium-to high-amplitude reflectors (**Figure 4A**). We correlate unit PQ with the Plio-Quaternary sedimentary succession widespread in the Tyrrhenian Sea based on its seismic signature and well log data.

Two subunits, named PL and LQ from bottom to top, were distinguished based on the occurrence of a well-defined unconformity that separates them (S1 in **Figures 4A**,**B**, **5A**,**B**). Well-seismic calibration indicates that the unconformity S1 formed during the Early Pleistocene (Calabrian).

Subunit PL is characterised by subparallel and well-defined laterally continuous reflectors with an aggradational internal pattern. The strata are sub-horizontal in the central and northern sectors of the line Sister-12 and show northwards directed onlap terminations onto the M horizon (**Figure 5A**). In the southern part of the seismic profile, reflectors exhibit a variable inclination from bottom to top, defining a fan geometry (FSD in **Figure 5A**). Subunit PL is also sub-horizontal in the southeastern sector of line ER-77-502, whereas it exhibits slightly seaward dipping reflections moving towards the north-west (**Figure 5B**).

The subunit LQ consists of a series of layered and generally sub-horizontal reflectors with an aggradational structure (**Figures 5A,B**). The strata terminate with onlap geometry onto the unconformity S1 in the central sector of the gulf (**Figures 4B**, **5A**, **6A**,**B**) and in the eastern one (**Figures 5B**, **7**). Conversely, strata paraconformably overlay subunits PL deposits towards both the north and the south. Another unconformity surface was detected within subunit LQ only in the southeastern sector of the Gulf, along the north-western flank of the Maida Ridge (S2 in **Figure 7**). Subunit LQ is bounded upwards by the seafloor.

The Sant'Eufemia Fault System

A series of normal faults that offset the deposits of Unit MD are observed on the high-penetration seismic profiles. Faults generally dip towards the south and bound horst (CDPs 1,250–1,500, **Figure 5A**) and half-graben (CDPs 1,600–2,300, **Figure 5A**) structures. Some faults are sealed by Pliocene deposits but younger activity is locally observed (e.g., CDPs 1800–2,100 in **Figure 5A**). In this area, the deposits of subunit PL show a fan-shaped geometry (FSD) with the thicker deposit in the hanging wall of a SSW-dipping fault (**Figure 5A**). We interpret these deposits as syn-tectonic strata associated with the development of a normal or transtensional fault that offset rocks deeper than 3 km (using 2000 m/s for the time to depth conversion). However, this fault shows a reverse feature in its upper part; thus, we interpret it as a

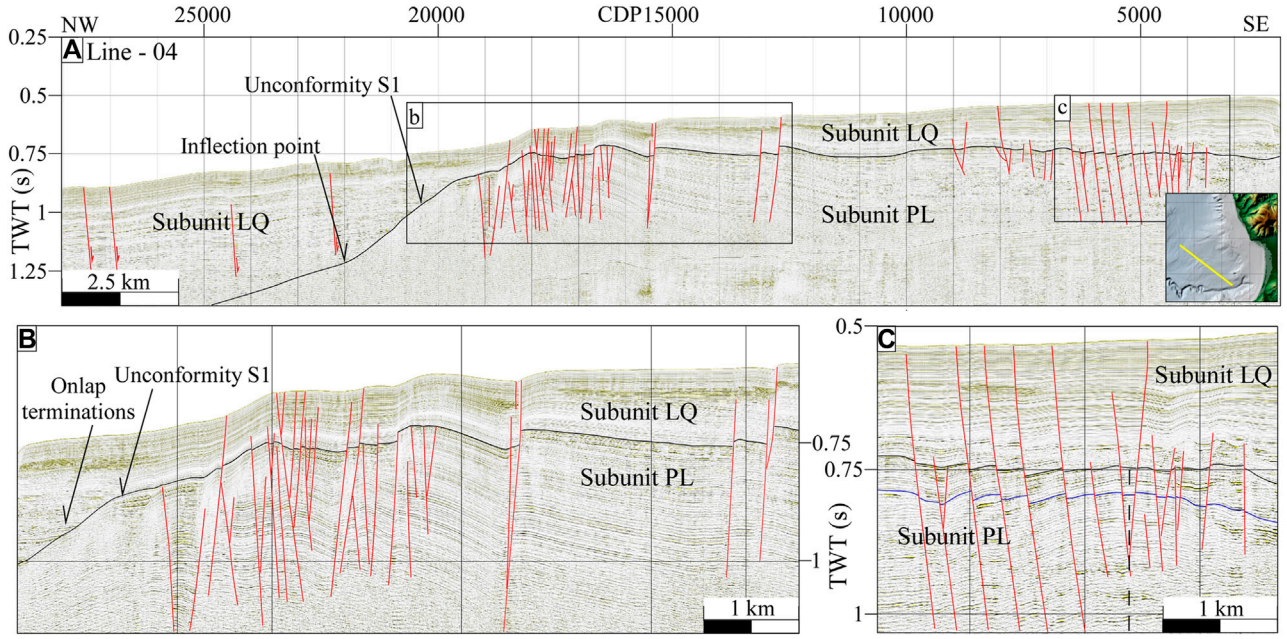

FIGURE 6 | (A) Seismic profile "Line—04" and its interpretation. Inset shows the location of the profile. **(B and C)** Parts of Line—04 that show high-angle trastensive faults. Blue line marks the south-westernmost part of the anticline associated to the development of the Maida Ridge. Black dashed line represents the anticline axis. Red lines indicate transtensional faults. PL and LQ are the subunits recognised in the Plio Quaternary deposits.

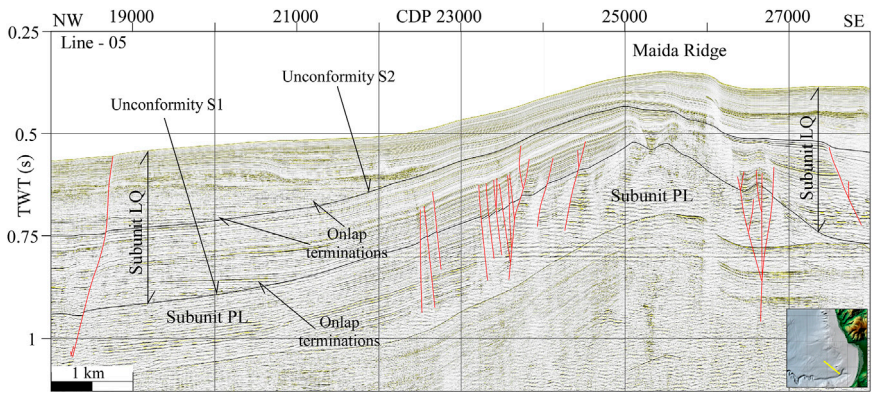

FIGURE 7 | Seismic profile "Line—05" and its interpretation. Inset shows the location of the profile. PL and LQ are the subunits recognised in the Plio Quaternary deposits. Red lines indicate transtensional faults.

positive inversion structure (probably due to transpression) involving subunit PL and older deposits. The inversion is partial (*sensu* Williams et al., 1989) because the deeper fault still retains an apparent normal displacement. Another positive partial inversion structure is observed towards the north (CDPs 1,500–1700 in **Figure 5A**). The transpressional reactivation of both faults leads to the uplift of the earlier basin fill and bending of the upper part of PL. Towards the east, sub-unit PL was also involved in shortening along steep transpressional ramps (**Figure 5B**). Seismic and well-log data suggest that the transpressional structures were active until the Calabrian. Thus, the unconformity S1 that limits the subunit PL deposits upward has a tectonic origin. Above this surface, LQ deposits show onlap reflectors terminating on top of unit PL (CDPs 1900–1950, **Figure 5A**).

The deep inversion structures involving subunit PL are not detectable on the high-resolution seismic profiles. Considering that the positive inversion structure was traced in correspondence of the inflection point of the unconformity S1 in the high-penetration seismic lines (**Figures 5A,B**), we used this inflection point to infer the shallow position of transpressional faults on the high-resolution seismic profiles (**Figure 6A**). In the central sector of the Sant'Eufemia Gulf, the transpressional faults show NE-SW orientations. NNE-SSW to NE-SW trending transpressional structures were also detected in the eastern

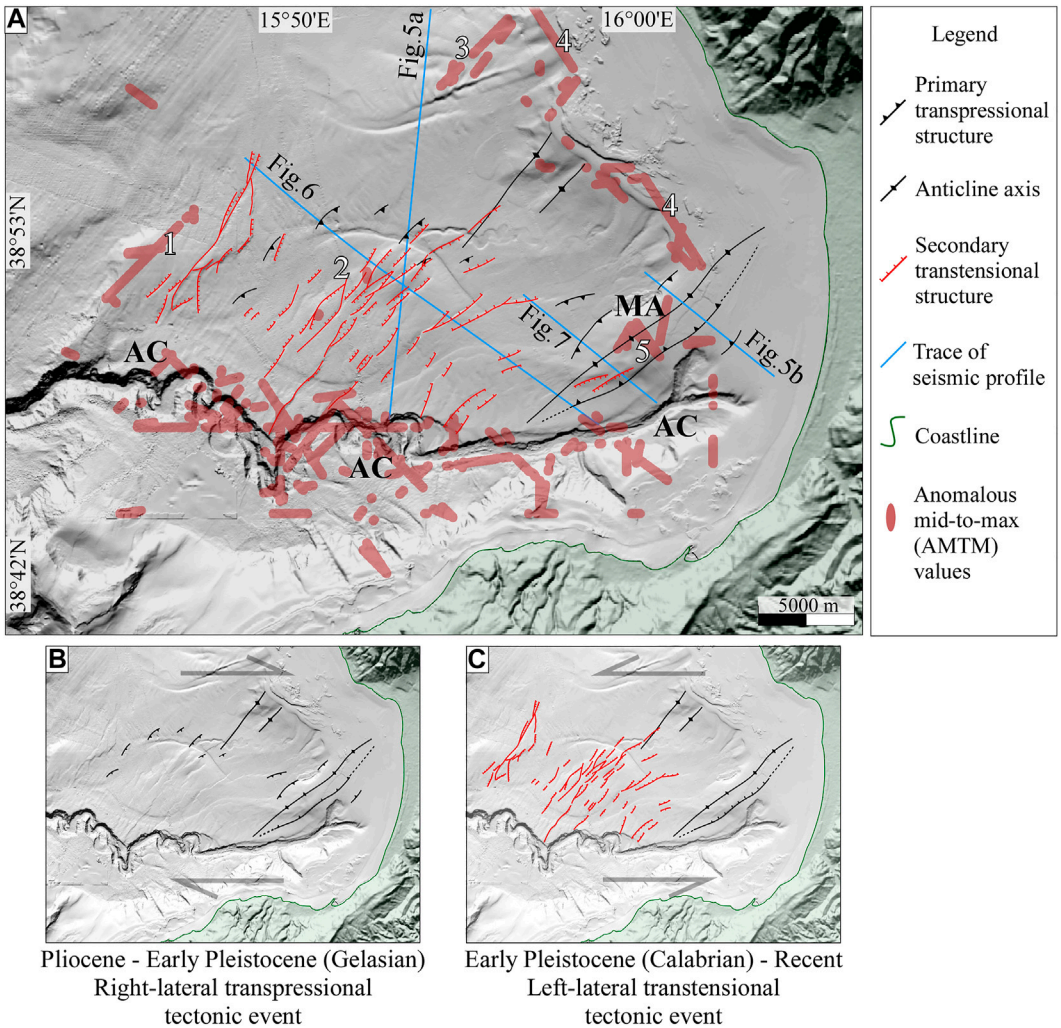

FIGURE 8 | (A) Structural map of the Sant'Eufemia Gulf. Red dots are the AMTM values localised at the intersection points of their related swath profiles. MA, Maida Ridge; AC, Angitola Canyon; 1, 2, 3, 4, and 5, sectors with alignments of AMTM values. **(B and C)** Schematic structural maps showing the active structures during the Pliocene—Early Pleistocene (Gelasian) and Early Pleistocene (Calabrian)—Recent tectonic events that affected the Sant'Eufemia Gulf. The activity of the structures is inferred from the analysis of seismic profiles and swath profiles (AMTM values).

sector of the Sant'Eufemia Gulf in correspondence with ridges (**Figures 3**, **5B**, **7**, **8A**). The most prominent structure is associated with the formation of the Maida Ridge (see *Morpho-Bathymetry Analysis*), and has a south-eastward asymmetric shape indicating its vergence (**Figures 7**, **8A**). A secondary unconformity S2 was identified along the north-western flank of this transpressional structure above the main unconformity S1 (**Figure 7**). The formation of this unconformity is probably linked to the tectonic activity of the structure associated with the development of the Maida Ridge.

NNE- SSW trending, closely-spaced, high-angle normal to transtensional faults offset the upper part of subunit PL and younger deposits (**Figures 6A–C**). Some of the faults reach the seafloor, whereas others propagate upwards, affecting the LQ deposits. The maximum depth at which these structures can be traced is generally less than 1.5 km (using 2000 m/s for the time to depth conversion). The transtensional faults show an anastomosing pattern in the central sector of the Sant'Eufemia Gulf, with individual segment length typically of a few km and rarely approaching 10 km (**Figure 8A**). Seafloor vertical offset along these faults vary from few meters to a few dozen meters, and, consequently, these faults have a mild morphological expression.

Morphotectonic Anomalies

The qualitative analysis of swath profiles shows morphological anomalies (relief anomalies, topography excesses, terraced surfaces, asymmetrical valleys, and counter-slope areas; **Figures 2E,F**) that suggest a transient landscape state due to a tectonic forcing.

The quantitative analysis of the swath profiles highlights AMTM values in distinct sectors of the gulf. In the western

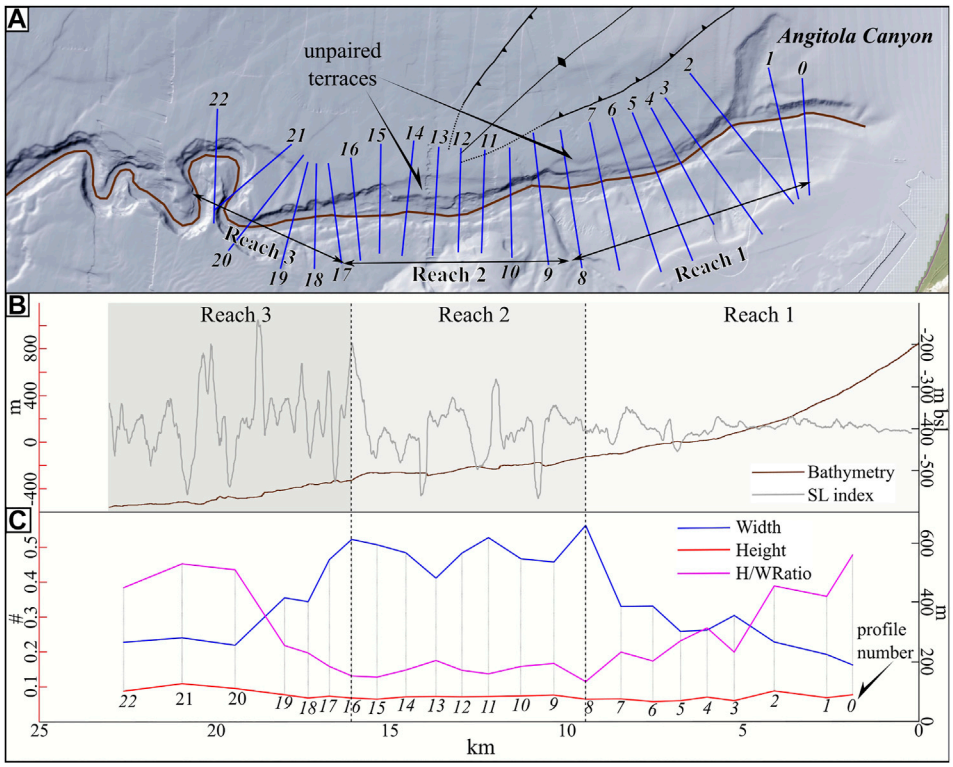

FIGURE 9 | A) Map view of the upstream portion of the Angitola Canyon. In black, the southern part of the Maida Ridge. In blue, the location of 23 bathymetric cross-profiles. In brown, the trace of the thalweg. The three double-arrowed black lines show the length of the three reaches. **(B)** The brown line and the black vertical axis relate to the long profile of the Angitola Canyon, while the grey curve and the red vertical axis represent the SL index computed values. **(C)** In red and blue, the canyon height and width curves, respectively; both curves refer to the black vertical axis. In magenta, the H/W ratio curve which values relate to the red vertical axis.

sector, an alignment of AMTM values is observed along a NE-SW morphological scarp (1 in **Figure 8A**). Few AMTM values were detected in the central sector of the gulf, whereas several alignments of AMTM were computed towards the east. In particular, AMTM values are observed in the north-eastern sector in correspondence of a roughly NE-SW striking bathymetric scarp (3 in **Figure 8A**) along the shelf-upper slope transition (4 in **Figure 8A**) and above the NE-SW trending transpressional Maida Ridge (5 in **Figure 8A**). Towards the south, many AMTM values are observed along the Angitola Canyon (AC in **Figure 8A**).

The longitudinal profile of the upper 22 km sublinear part of the thalweg of the Angitola Canyon and the cross profiles allowed the detection of three different reaches characterised by different Stream Length-gradient (SL) index and H/W values and trends (**Figures 9A,B**). The roughly constant negative trend of H/W and the correlative flat SL trend (avg. 125, st. dev. of 52), extending from the canyon head to roughly 9 km, describes the steady-state and concave upward shape of the Reach 1 of the profile (**Figures 9A,B**). The average canyon width is roughly 303 m, and its standard deviation is about 72 m. We detect the minimum SL (avg. 116, st. dev. 187) and H/W values in Reach 2, ranging from 9 to 16 km (**Figure 9C**). Such low values, corresponding to an average width of 574 m (st. dev. 90 m), can be interpreted as an increase of the canyon width relative to its height or a change to a less erodible bedrock of the thalweg. Differently, a positive trend of the H/W curve and a high-amplitude SL curve (avg. 826, st. dev. 1,308) distinguish Reach 3, extending till the first meander that characterises the deeper part of the Angitola Canyon.

The positive trend of the H/W curve of the Reach 3, together with the average canyon heights (~81, 83 and 100 m with a standard deviation of 7, 4, and 17 m for Reach 1, Reach 2 and Reach 3, respectively), highlights a growing stream power moving towards the canyon outlet.

DISCUSSION

From Deep to Shallow: Tectonic Interpretation of the Sant'Eufemia Gulf

The structural investigation results integrated with the geomorphic analysis pinpoint three major tectonic events in the structural evolution of the Sant'Eufemia Gulf from Late Miocene to Recent times. We propose to frame these tectonic events within the kinematics of a deep-seated slab tear drawn from previous geodynamic analysis of the region (Lucente et al., 1999; Rosenbaum et al., 2008) and interpreted as a regional, first-order structure.

Seismic reflection profiles show that the first tectonic event was characterised by the development of extensional faults during

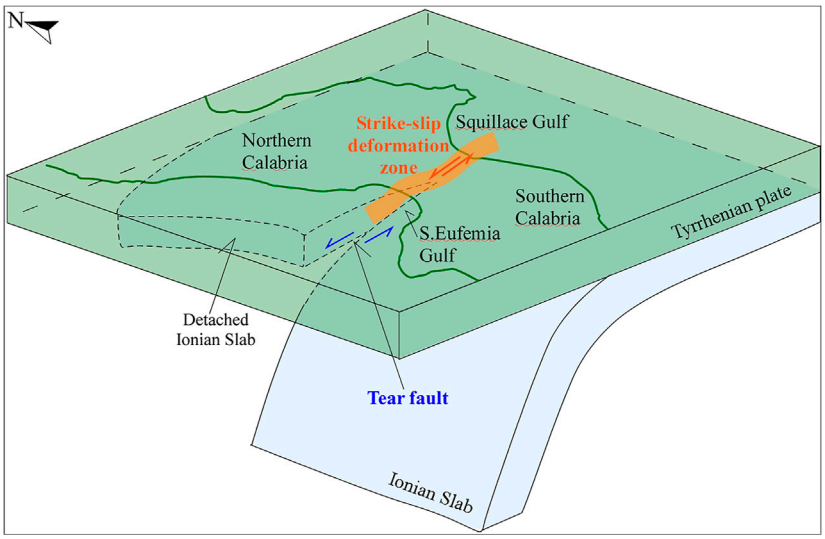

FIGURE 10 | Geodynamic sketch of the Tyrrhenian-Ionian subduction system illustrating the strike-slip deformation zone extending from Sant'Eufemia Gulf to Squillace Gulf formed above the tear fault inferred between two segments of the Ionian slab.

the Late Miocene (**Figure 5A**). The second tectonic event was characterised by the positive inversion of deep (>3 km) extensional faults inherited from the previous event (**Figure 5A**). During this stage, we also document the formation of transpressional faults and NNE-SSW to NE-SW oriented anticlines (e.g., the Maida Ridge), involving Upper Miocene to Lower Pleistocene (Gelasian) deposits, in the central and eastern sector of the gulf, respectively (**Figures 5B**, **8A**,**B**). The orientation of the anticlines and their en-echelon arrangement suggest that they developed within a roughly E-W oriented right-lateral transpressional zone, located above the deep-seated slab tear fault (red line in **Figure 1D**). The last tectonic event began in the Early Pleistocene (Calabrian). It was characterised by the onset of shallow (less than 1.5 km), NNE- SSW trending, high-angle normal to oblique faults (**Figures 5A**, **6**, **7**). The orientation of these younger faults (**Figures 8A,C**) suggests that they formed in a left-lateral strike-slip regime along the E-W oriented shear zone. This interpretation is consistent with the deep-seated structural setting documented by Guarnieri, 2006, suggesting a current left-lateral wrenching develops between Sant'Eufemia Gulf and Squillace Gulf, and with seismological data that highlight left-lateral focal mechanisms in this sector of Calabria (e.g., Presti et al., 2013).

Data and interpretation highlight a change from right-lateral to left-lateral kinematic since the Calabrian. A kinematic change for the second and third tectonic event was proposed by Brutto et al. (2016) based on field data collected in the western Catanzaro Trough and on the interpretation of seismic profiles collected in the Sant'Eufemia Gulf. Conversely, the evolutionary model proposed by Brutto et al. (2016) suggests that the last extensional stage is governed by a sub-vertical P-axis similarly to what occurs slightly to the south, from the Messina Straits to the Mesima Valley. In the northern sector of the Catanzaro Trough and adjacent Squillace Gulf, an ESE-WNW trending strike-slip fault system (**Figures 1A,E**; Lamezia-Catanzaro line, Tansi et al., 2007) and an E-W trending transtensional basin connected to a negative flower structure (Del Ben et al., 2008) developed since the Late Miocene, respectively. The strike-slip fault system offsets the Middle Miocene to Lower Pleistocene deposits on-land (van Dijk et al., 2000; Tansi et al., 2007) and Plio-Quaternary sequences in the Squillace Gulf (Del Ben et al., 2008). Their orientation confirms that a roughly E-W oriented crustal strike-slip fault can be traced from the Sant'Eufemia Gulf to the Squillace Gulf. On a lithospheric scale, the western part of the crustal fault lies over an ESE-WNW trending, shallow (<100 km) slab tear fault (red line in **Figure 1D**, Rosenbaum et al., 2008). Because a slab tear fault develops in the correspondence of two adjacent parts of the lower plate that move at different rollback velocities (Rosenbaum et al., 2008), the formation of the crustal faults can be considered as the upper plate response to the tearing of the lower plate (**Figure 10**). Considering the age of the older deposits affected by the upper plate deformation, we infer that the formation of the tear fault started in the Late Miocene.

The slip-sense inversion from right-lateral to left-lateral of the roughly E-W oriented crustal strike-slip fault traced from the Sant'Eufemia Gulf to the Squillace Gulf could be the result of a deceleration of the eastward motion of the northern part of the Calabrian Arc with respect to the southern sector during the Quaternary transition from the tectonic event 2 – 3, as a consequence of the collision of the northern sector of the Calabrian Arc with the continental crust of the Apulian foreland (Guarnieri, 2006). This event has partially inhibited the propagation of the northern part with respect to the southern sector that continued to migrate southeastwards (**Figure 10**). The same effect could have resulted from the slab detachment (~700 ka) that caused the end of the subduction

beneath the northern Calabrian Arc (Neri et al., 2009; Scarfì et al., 2018).

Landscape Response of the Sant'Eufemia Gulf to Tectonic Forcing

The alignment of the AMTM values in correspondence with a NE-SW seafloor scarp developed in the western sector of the gulf (1 in **Figure 8A**) suggests a recent morphostructural control on its formation. The geometrical and stereological characteristics of this N15°E striking, 10 km long and 200 m high scarp, make this morphological feature compatible with the deep structures detected on the high-penetration seismic profiles.

A few AMTM values were detected in the central sector of the Gulf (2 in **Figure 8A**), where a number of NNE-SSW-trending shallow normal to transtensional faults offset the seafloor. The limited occurrence of AMTM values indicates that the wavelength of the topographic signature of the normal to transtensional faults is smaller than the width of the swath profiles. Thus, the morphometric analysis confirms that these faults are basically shallow structures, whose roots do not reach the same depth as the transpressional faults. No AMTM values were found in correspondence to the deep transpressional faults in the central sector of the Gulf, suggesting that this structure is probably inactive.

In the eastern sector of the Gulf, AMTM values were detected in correspondence of the NNE-SSW to NE-SW trending anticlines (e.g., Maida Ridge, MA in **Figure 8A**), indicating that these structures controlled the morphology of the eastern sector of the Gulf in recent times. Thus, the analysis of swath profiles suggests that deep transpressional faults (e.g., CDPs 260–300 in **Figure 5B**), associated with the development of the anticlines during the second tectonic event (see *From Deep to Shallow*: *Tectonic Interpretation of the Sant'Eufemia Gulf*), were reactive in the left-lateral transtensional regime that characterises the last tectonic event.

In the southern sector of the Gulf, several AMTM values are detected along the Angitola Canyon. However, in this case, the tectonic forcing probably has triggered multiple geomorphological processes (e.g., gravitational processes, changes in slope and drainage patterns, sediment density flows that travel down the canyon, etc.) able to produce AMTM values. Thus, we have integrated the analysis of swath profiles with the bathymetric analysis of the Angitola Canyon to better understand the possible tectonic forcing of the 22 km long upstream section of the channel. The longitudinal profile of the canyon (**Figure 9**) shows that Reach 1 follows a steady-state evolution process as attested by its concave upward bathymetric profile and the flat SL trend. Along Reach 1, the canyon progressively increases its width in the downstream direction and approaches the Maida Ridge. Reach 2 responds to a tectonic landward tilt process and to the lateral tectonic forcing, as shown by the minimum SL value, the maximum width of the channel, and the corresponding minimum value of the H/W ratio associated with a steady H value. Finally, the morphology of the Reach 3 evolves following a growing stream power, as inferred by higher SL values and an increasing H/W ratio.

The change in the longitudinal slope of the canyon between Reach 2 and Reach 3 and the asymmetric shape of the canyon, expressed by the active channel flowing near the southern wall and the presence of unpaired terraces along the northern flank (**Figure 9A**), suggest that Reach 2 and Reach 3 underwent differential uplift. Considering that the south-western prolongation of the Maida Ridge roughly lies below the boundary between the Reach 2 and Reach 3 of the canyon, we infer that the differential uplift of the two reaches represents the topographic response to the Late Quaternary activity of the Maida Ridge.

Seismotectonic Implications

The 1905 earthquake, one of the largest seismic event in Italy, was widely felt along the whole Tyrrhenian coastline of Calabria, with maximum macroseismic intensities documented in the northern part of the Capo Vaticano promontory (CFTI5Med, Guidoboni et al., 2018; CPTI15, Rovida et al., 2021). The earthquake also triggered a tsunami wave that flooded the coastline of central Calabria (Piatanesi and Tinti, 2002; Loreto et al., 2017; Maramai et al., 2019). Shaking scenarios suggest that the seismogenic fault is located in the Sant'Eufemia Gulf (Sandron et al., 2015). Two different structures located south of the Capo Vaticano promontory (Cucci and Tertulliani 2010) and in the Sant'Eufemia Gulf (Loreto et al., 2013) were proposed as seismogenic faults. The different hypothesis on the source of the 1905 seismic event is due to the difficulty of identifying offshore structural lineaments able to produce high-magnitude seismic events.

Some consideration on the age and stratigraphy of the deformed units is necessary to infer the seismogenic potential of the two sets of faults mapped in the Sant'Eufemia Gulf. The Pliocene to Early Pleistocene (Calabrian) transpressional faults (primary fault set) deform highly competent rocks of the Kabilian-Calabrian units, including imbricate sheets of the Hercynian basement, Alpine poly-metamorphic rocks, and Mesozoic sedimentary units. Conversely, the faults of the shallower transtensional deformation zone (secondary fault set) dissect less competent Pliocene fine-grained (mudstone and claystone) and Quaternary coarser (sandstone and siltstone) rocks. Based on the depth and geometry of the faults (i.e., dimension derived from mapped fault length and width) and on the lithology of the deformed rocks, we suggest that the potential source of large magnitude earthquakes should be related to the primary fault set.

The anticline axis of the Maida Ridge was mapped for a length of about 15 km (MA in **Figure 8A**). This value is probably underestimated due to the lack of seismic data at the NE and SW terminations of the structure, close to the coastline and the Angitola Canyon, respectively. Geomorphic analysis of the upper reach of the canyon indicates that its evolution was controlled by tectonic forcing compatible with the growth of the anticline. Thus, the length of the deep fault, associated with the development of the anticline, possibly extends south-westward for an additional 3–4 km. The deep structure evolved during the second tectonic stage (Pliocene - Gelasian) as a transpressional fault (**Figures 5B**, **8B**).

Successively, it was active during the last tectonic event (Calabrian—Recent, **Figure 8C**) in a left-lateral transtensional regime, as suggested by 1) the distribution of the AMTM values indicating that the tectonic activity of the deep fault, responsible for the formation of the Maida Ridge, controlled the seafloor morphology in recent time (see *Landscape Response of the Sant'Eufemia Gulf to Tectonic Forcing*), 2) the bathymetric analysis of the upper reach of the Angitola Canyon indicating that the growth of the Maida Ridge controlled the evolution of the canyon in the Late Quaternary (see *Landscape Response of the Sant'Eufemia Gulf to Tectonic Forcing*), and 3) the NNE-SSW orientation of the deep fault that is compatible with its reactivation in a left-lateral transtensional regime (see *Landscape Response of the Sant'Eufemia Gulf to Tectonic Forcing*, **Figure 8C**). Considering the length and depth of this deep fault, its recent activity, and its location close to the epicentre of the 1905 event as inferred by Camassi et al. (1997) (red square-3 in **Figure 1F**), we suggest that the deep primary fault, associated with the growth of the Maida Ridge, is likely the seismogenic source of the 1905 earthquake.

The seismogenic fault proposed by Loreto et al. (2013); Brutto et al. (2016) (SEF in **Figure 1E**, included in the DISS database as the "ITIS139 Sant'Eufemia", DISS Working Group, 2018) is an extensional, SE-dipping fault, formed along the southeastern flank of the Maida Ridge. This fault offsets shallow reflectors (at a depth less than 2 s, Figure 13 in Brutto et al., 2016). Based on its depth and its direction, parallel to the shallow transtensional faults documented in our study, we interpret this fault as a secondary structure.

Our suggested seismogenic fault also differs from an intra-plate rupture at the bending zone of the Ionian subduction slab, proposed by Presti et al. (2017), that implies a deeper seismogenic source at a depth of several tens of kilometres. However, the tectonic model we suggest does not exclude the formation of a structure in the subducting lithosphere of the lower plate along or near the slab tear fault.

CONCLUSION

A multiscale approach based on the interpretation of multichannel seismic profiles with different resolution/penetration and quantitative morphometric analysis of multibeam bathymetry provides new insights into the characterisation of active faults in offshore areas. The results of this work allowed to reconstruct the structural setting and the kinematic evolution of surficial and deeper faults developed in the Sant'Eufemia Gulf (Tyrrhenian offshore of the Calabrian Arc) since the Late Miocene, and to detect their morphological signature at the seafloor. The main conclusions can be summarised as follows:

1. Three tectonic events controlled the evolution of the Sant'Eufemia Gulf since the Late Miocene. The first one is an extensional or transtensional phase that occurred during the Late Miocene. Following, a right-lateral transpressional tectonic event developed from the Early Pliocene to the Early Pleistocene. It caused the positive inversion of deep (>3 km) extensional/transtensional tectonic features and the formation of NNE-SSW to NE-SW trending anticlines (e.g., Maida Ridge). Since the Early Pleistocene (Calabrian), a left-lateral transtensional regime induced the formation of shallow (less than 1.5 km), NNE-SSW oriented, high-angle normal to transtensional faults.
2. The integration of seismic reflection and quantitative morphometric analysis provides evidence that the NNE-SSW to NE-SW trending anticlines, formed during the Pliocene to Early Pleistocene (Gelasian), were reactivated during the Calabrian to Recent left-lateral transtensional event. Also, the bathymetric analysis of the Angitola Canyon suggests a differential uplift between two reaches of the canyon. We infer that the south-western prolongation of the Maida Ridge lies below the canyon and, thus, the differential uplift may be regarded as a topographic response of the Late Quaternary negative inversion of the fault that has controlled the growth of the Maida Ridge.
3. Based on the length (>15 km), and recent tectonic activity, the deep structure controlling the development of the Maida Ridge can be considered a potential candidate for the seismogenic source of the 1905 earthquake.
4. Our results, integrated with previous literature, support the hypothesis that the transpressional/transtensional structures detected in the study area correspond to a ~E-W oriented crustal strike-slip fault zone extending from the Sant'Eufemia Gulf to Squillace Basin (Ionian Sea). This zone may be regarded as a crustal response to the development of a tear fault in the lower plate.

DATA AVAILABILITY STATEMENT

The original contributions presented in the study are included in the article/Supplementary Material, further inquiries can be directed to the corresponding author.

AUTHOR CONTRIBUTIONS

MC and FP conceived the study, carried out the seismic data set interpretation and drew up the manuscript. PB and NP conceived the study, carried out the qualitative and quantitative morphometric analysis of multibeam data and drew up the manuscript. MK contributed to the acquisition of the high-resolution multichannel seismic data, carried out their interpretation and revised the manuscript. AB, DC, and EM, performed the acquisition, processing, analysis and interpretation of the high-resolution multibeam bathymetry data and revised the manuscript. GB, LF, CM, and MS, discussed the data set and revised the manuscript. GT contributed to the acquisition of the High-Resolution multichannel seismic data and revised the manuscript.

FUNDING

This study has been partly funded by the joint projects of Ministero degli Affari Esteri e della Cooperazione Internazionale in collaboration with the Israeli Ministry of Science and Technology grant no. 3-14333 in the frame of the EPAF Project (principal investigators FP and MK) and MUSE 4D-Overtime tectonic, dynamic and rheologic control on destructive multiple seismic events -Special Italian Faults and Earthquakes: From real 4-D cases to models, in the frame of PRIN 2017. High resolution multichannel seismic reflection data (Geo-Source Sparker) were acquired by the "Geo Marine Survey Systems" company (Rotterdam, Netherlands) and processed by the "GeoSurvey" company (Aveiro, Portugal). Interpretation of seismic profiles was performed within the GeoSuite AllWork software package. Bathymetric data were collected in research projects funded by the National Research Council.

ACKNOWLEDGMENTS

We acknowledge AZ, an reviewer and the associate editor PV for their critical reading and useful comments that allowed us to improve the manuscript.

REFERENCES

Argnani, A. (2009). Evolution of the Southern Tyrrhenian Slab Tear and Active Tectonics along the Western Edge of the Tyrrhenian Subducted Slab. *Geol. Soc. Lond. Spec. Publications* 311, 193–212. doi:10.1144/sp311.7

Baes, M., Govers, R., and Wortel, R. (2011). Subduction Initiation along the Inherited Weakness Zone at the Edge of a Slab: Insights from Numerical Models. *Geophys. J. Int.* 184, 991–1008. doi:10.1111/j.1365-246x.2010.04896.x

Barreca, G., Bruno, V., Cocorullo, C., Cultrera, F., Ferranti, L., Guglielmino, F., et al. (2014). Geodetic and Geological Evidence of Active Tectonics in South-Western Sicily (Italy). *J. Geodynamics* 82, 138–149. doi:10.1016/j.jog.2014.03.004

Barreca, G., Corradino, M., Monaco, C., and Pepe, F. (2018). Active Tectonics along the South East Offshore Margin of Mt. Etna: New Insights from High-Resolution Seismic Profiles. *Geosciences* 8, 62. doi:10.3390/geosciences8020062

Billi, A., Barberi, G., Faccenna, C., Neri, G., Pepe, F., and Sulli, A. (2006). Tectonics and Seismicity of the Tindari Fault System, Southern Italy: Crustal Deformations at the Transition between Ongoing Contractional and Extensional Domains Located above the Edge of a Subducting Slab. *Tectonics* 25. doi:10.1029/2004tc001763

Bonardi, G., Cavazza, W., Perrone, V., and Rossi, S. (2001). "Calabria-Peloritani Terrane and Northern Ionian Sea," in *Anatomy of an Orogen: The Apennines and Adjacent Mediterranean Basins* (Springer), 287–306. doi:10.1007/978-94-015-9829-3_17

Bonini, L., Bucci, D. D., Toscani, G., Seno, S., and Valensise, G. (2011). Reconciling Deep Seismogenic and Shallow Active Faults through Analogue Modelling: the Case of the Messina Straits (Southern Italy). *J. Geol. Soc.* 168, 191–199. doi:10.1144/0016-76492010-055

Brutto, F., Muto, F., Loreto, M. F., Paola, N. D., Tripodi, V., Critelli, S., et al. (2016). The Neogene-Quaternary Geodynamic Evolution of the central Calabrian Arc: A Case Study from the Western Catanzaro Trough basin. *J. Geodynamics* 102, 95–114. doi:10.1016/j.jog.2016.09.002

Burbank, D. W., and Anderson, R. S. (2011). *Tectonic Geomorphology*. Wiley Online Library. doi:10.1002/9781444345063Available at: http://search.ebscohost.com/login.aspx?direct=true&db=edsebk&AN=408384&site=eds-live

Camassi, R., Stucchi, M., and Molin, D. (1997). *NT4. 1 un catalogo parametrico di terremoti di area italiana al di sopra della soglia del danno*. Terremoti, Milano: Consiglio Nazionale delle Richerche, Gruppo Nazionale per la Difesa dai.

Carafa, M. M. C., Kastelic, V., Bird, P., Maesano, F. E., and Valensise, G. (2018). A "Geodetic Gap" in the Calabrian Arc: Evidence for a Locked Subduction Megathrust?. *Geophys. Res. Lett.* 45, 1794–1804. doi:10.1002/2017GL076554

Carminati, E., and Doglioni, C. (2005). EUROPE | Mediterranean Tectonics. *Encycl. Geol.* 2, 135–146. doi:10.1016/b0-12-369396-9/00135-0

Carminati, E., Wortel, M. J. R., Spakman, W., and Sabadini, R. (1998). The Role of Slab Detachment Processes in the Opening of the Western-central Mediterranean Basins: Some Geological and Geophysical Evidence. *Earth Planet. Sci. Lett.* 160, 651–665. doi:10.1016/S0012-821X(98)00118-6

Chatelain, J.-L., Molnar, P., Prévot, R., and Isacks, B. (1992). Detachment of Part of the Downgoing Slab and Uplift of the New Hebrides (Vanuatu) Islands. *Geophys. Res. Lett.* 19, 1507–1510. doi:10.1029/92gl01389

Chiarabba, C., De Gori, P., and Mele, F. M. (2015). Recent Seismicity of Italy: Active Tectonics of the central Mediterranean Region and Seismicity Rate Changes after the Mw 6.3 L'Aquila Earthquake. *Tectonophysics* 638, 82–93. doi:10.1016/j.tecto.2014.10.016

Chiarabba, C., De Gori, P., and Speranza, F. (2008). The Southern Tyrrhenian Subduction Zone: Deep Geometry, Magmatism and Plio-Pleistocene Evolution. *Earth Planet. Sci. Lett.* 268, 408–423. doi:10.1016/j.epsl.2008.01.036

Chiarabba, C., and Palano, M. (2017). Progressive Migration of Slab Break-Off along the Southern Tyrrhenian Plate Boundary: Constraints for the Present Day Kinematics. *J. Geodynamics* 105, 51–61. doi:10.1016/j.jog.2017.01.006

Corradino, M., Pepe, F., Bertotti, G., Picotti, V., Monaco, C., and Nicolich, R. (2020). 3-D Architecture and Plio-Quaternary Evolution of the Paola Basin: Insights into the Forearc of the Tyrrhenian-Ionian Subduction System. *Tectonics* 39. doi:10.1029/2019tc005898

Corradino, M., Pepe, F., Sacchi, M., Solaro, G., Duarte, H., Ferranti, L., et al. (2021). Resurgent Uplift at Large Calderas and Relationship to Caldera-Forming Faults and the Magma Reservoir: New Insights from the Neapolitan Yellow Tuff Caldera (Italy). *J. Volcanol. Geotherm. Res.* 411, 107183. doi:10.1016/j.jvolgeores.2021.107183

Cosentino, C., Molisso, F., Scopelliti, G., Caruso, A., Insinga, D. D., Lubritto, C., et al. (2017). Benthic Foraminifera as Indicators of Relative Sea-Level Fluctuations: Paleoenvironmental and Paleoclimatic Reconstruction of a Holocene marine Succession (Calabria, South-Eastern Tyrrhenian Sea). *Quat. Int.* 439, 79–101. doi:10.1016/j.quaint.2016.10.012

Cucci, L., and Tertulliani, A. (2010). The Capo Vaticano (Calabria) Coastal Terraces and the 1905 M7 Earthquake: the Geomorphological Signature of Regional Uplift and Coseismic Slip in Southern Italy. *Terra Nova* 22 (5), 378–389. doi:10.1111/j.1365-3121.2010.00961.x

Cultrera, F., Barreca, G., Burrato, P., Ferranti, L., Monaco, C., Passaro, S., et al. (2017b). Active Faulting and continental Slope Instability in the Gulf of Patti (Tyrrhenian Side of NE Sicily, Italy): A Field, marine and Seismological Joint Analysis. *Nat. Hazards* 86, 253–272. doi:10.1007/s11069-016-2547-y

Cultrera, F., Barreca, G., Ferranti, L., Monaco, C., Pepe, F., Passaro, S., et al. (2017a). Structural Architecture and Active Deformation Pattern in the Northern Sector of the Aeolian-Tindari-Letojanni Fault System (SE Tyrrhenian Sea-NE Sicily) from Integrated Analysis of Field, marine Geophysical, Seismological and Geodetic Data. *Ijg* 136 (3), 399–417. doi:10.3301/IJG.2016.17

De Ritis, R., Pepe, F., Orecchio, B., Casalbore, D., Bosman, A., Chiappini, M., et al. (2019). Magmatism along Lateral Slab Edges: Insights from the Diamante-Enotrio-Ovidio Volcanic-Intrusive Complex (Southern Tyrrhenian Sea). *Tectonics* 38, 2581–2605. doi:10.1029/2019tc005533

De Ritis, R., Ventura, G., Chiappini, M., Carluccio, R., and von Frese, R. (2010). Regional Magnetic and Gravity Anomaly Correlations of the Southern Tyrrhenian Sea. *Phys. Earth Planet. Interiors* 181, 27–41. doi:10.1016/j.pepi.2010.04.003

Del Ben, A., Barnaba, C., and Taboga, A. (2008). Strike-slip Systems as the Main Tectonic Features in the Plio-Quaternary Kinematics of the Calabrian Arc. *Mar. Geophys. Res.* 29, 1–12. doi:10.1007/s11001-007-9041-6

Devoti, R., D'Agostino, N., Serpelloni, E., Pietrantonio, G., Riguzzi, F., Avallone, A., et al. (2017). A Combined Velocity Field of the Mediterranean Region. *Ann. Geophys.* 60, S0215. doi:10.4401/ag-7059

Di Bucci, D., Ridente, D., Fracassi, U., Trincardi, F., and Valensise, G. (2009). Marine Palaeoseismology from Very High Resolution Seismic Imaging: the Gondola Fault Zone (Adriatic Foreland). *Terra Nov* 21, 393–400. doi:10.1111/j.1365-3121.2009.00895.x

DISS Working Group (2018). Database of Individual Seismogenic Sources (DISS), Version 3.2.1: A Compilation of Potential Sources for Earthquakes Larger Than M 5.5 in Italy and Surrounding Areas. Available at: http://diss.rm.ingv.it/diss/, Istituto Nazionale di Geofisica e Vulcanologia. doi:10.6092/INGV.IT-DISS3.2.1

Doglioni, C., Innocenti, F., and Mariotti, G. (2001). Why Mt Etna?. *Terra Nova* 13, 25–31. doi:10.1046/j.1365-3121.2001.00301.x

Faccenna, C., Becker, T. W., Lucente, F. P., Jolivet, L., and Rossetti, F. (2001). History of Subduction and Back-Arc Extension in the central Mediterranean. *Geophys. J. Int.* 145, 809–820. doi:10.1046/j.0956-540X.2001.01435.x

Faccenna, C., Funiciello, F., Civetta, L., D Antonio, M., Moroni, M., and Piromallo, C. (2007). Slab Disruption, Mantle Circulation, and the Opening of the Tyrrhenian Basins. *Spec. Pap. Soc. Am.* 418, 153. doi:10.1130/2007.2418(08)

Ferranti, L., Burrato, P., Pepe, F., Santoro, E., Mazzella, M. E., Morelli, D., et al. (2014). An Active Oblique-Contractional belt at the Transition between the Southern Apennines and Calabrian Arc: The Amendolara Ridge, Ionian Sea, Italy. *Tectonics* 33, 2169–2194. doi:10.1002/2014TC003624

Ferranti, L., Santoro, E., Mazzella, M. E., Monaco, C., and Morelli, D. (2009). Active Transpression in the Northern Calabria Apennines, Southern Italy. *Tectonophysics* 476, 226–251. doi:10.1016/j.tecto.2008.11.010

Fracassi, U., Di Bucci, D., Ridente, D., Trincardi, F., and Valensise, G. (2008). *Activity of the Gondola Fault Zone and Potential Earthquake Sources Offshore the Gargano Promontory (Adriatic Sea)*.

Gallais, F., Graindorge, D., Gutscher, M.-A., and Klaeschen, D. (2013). Propagation of a Lithospheric Tear Fault (STEP) through the Western Boundary of the Calabrian Accretionary Wedge Offshore Eastern Sicily (Southern Italy). *Tectonophysics* 602, 141–152. doi:10.1016/j.tecto.2012.12.026

Galli, P. A. C., and Peronace, E. (2015). Low Slip Rates and Multimillennial Return Times for Mw 7 Earthquake Faults in Southern Calabria (Italy). *Geophys. Res. Lett.* 42 (13), 5258–5265. doi:10.1002/2015gl064062

Galli, P., and Molin, D. (2009). Il terremoto del 1905 in Calabria: Revisione della distribuzione degli effetti e delle ipotesi sismogenetiche. *Quat. Ital. J. Quat. Sci.* 22, 207–234.

Govers, R., and Wortel, M. J. R. (2005). Lithosphere Tearing at STEP Faults: Response to Edges of Subduction Zones. *Earth Planet. Sci. Lett.* 236, 505–523. doi:10.1016/j.epsl.2005.03.022

Guarnieri, P. (2006). Plio-Quaternary Segmentation of the South Tyrrhenian Forearc basin. *Int. J. Earth Sci. (Geol Rundsch)* 95, 107–118. doi:10.1007/s00531-005-0005-2

Guidoboni, E., Ferrari, G., Mariotti, D., Comastri, A., Tarabusi, G., Sgattoni, G., et al. (2018). *CFTI5Med, Catalogo dei Forti Terremoti in Italia (461 aC-1997) e nell'area Mediterranea (760 aC-1500)*.

Guidoboni, E., Ferrari, G., Mariotti, D., Comastri, A., Tarabusi, G., and Valensise, G. (2007). *Catalogue of Strong Earthquakes in Italy (461 BC-1997) and Mediterranean Area (760 BC-1500)*.

Gutscher, M.-A., Dominguez, S., De Lepinay, B. M., Pinheiro, L., Gallais, F., Babonneau, N., et al. (2016). Tectonic Expression of an Active Slab Tear from High-Resolution Seismic and Bathymetric Data Offshore Sicily (Ionian Sea). *Tectonics* 35, 39–54. doi:10.1002/2015TC003898

Gutscher, M.-A., Kopp, H., Krastel, S., Bohrmann, G., Garlan, T., Zaragosi, S., et al. (2017). Active Tectonics of the Calabrian Subduction Revealed by New Multi-Beam Bathymetric Data and High-Resolution Seismic Profiles in the Ionian Sea (Central Mediterranean). *Earth Planet. Sci. Lett.* 461, 61–72. doi:10.1016/j.epsl.2016.12.020

ISIDe Working Group (2007). *Italian Seismological Instrumental and Parametric Database (ISIDe)*. Istituto Nazionale di Geofisica e Vulcanologia (INGV). doi:10.13127/ISIDE

Knott, S. D., and Turco, E. (1991). Late Cenozoic Kinematics of the Calabrian Arc, Southern Italy. *Tectonics* 10, 1164–1172. doi:10.1029/91tc01535

Lallemand, S., Font, Y., Bijwaard, H., and Kao, H. (2001). New Insights on 3-D Plates Interaction Near Taiwan from Tomography and Tectonic Implications. *Tectonophysics* 335, 229–253. doi:10.1016/s0040-1951(01)00071-3

Levin, V., Shapiro, N., Park, J., and Ritzwoller, M. (2002). Seismic Evidence for Catastrophic Slab Loss beneath Kamchatka. *Nature* 418, 763–767. doi:10.1038/nature00973

Loreto, M. F., Fracassi, U., Franzo, A., Del Negro, P., Zgur, F., and Facchin, L. (2013). Approaching the Seismogenic Source of the Calabria 8 September 1905 Earthquake: New Geophysical, Geological and Biochemical Data from the S. Eufemia Gulf (S Italy). *Mar. Geology.* 343, 62–75. doi:10.1016/j.margeo.2013.06.016

Loreto, M. F., Pagnoni, G., Pettenati, F., Armigliato, A., Tinti, S., Sandron, D., et al. (2017). Reconstructed Seismic and Tsunami Scenarios of the 1905 Calabria Earthquake (SE Tyrrhenian Sea) as a Tool for Geohazard Assessment. *Eng. Geology.* 224, 1–14. doi:10.1016/j.enggeo.2017.04.018

Loreto, M. F., Pepe, F., De Ritis, R., Ventura, G., Ferrante, V., Speranza, F., et al. (2015). Geophysical Investigation of Pleistocene Volcanism and Tectonics Offshore Capo Vaticano (Calabria, southeastern Tyrrhenian Sea). *J. Geodynamics* 90, 71–86. doi:10.1016/j.jog.2015.07.005

Loreto, M. F., Zitellini, N., Ranero, C. R., Palmiotto, C., and Prada, M. (2021). Extensional Tectonics during the Tyrrhenian Back-arc basin Formation and a New Morpho-tectonic Map. *Basin Res.* 33, 138–158. doi:10.1111/bre.12458

Lucente, F. P., Chiarabba, C., Cimini, G. B., and Giardini, D. (1999). Tomographic Constraints on the Geodynamic Evolution of the Italian Region. *J. Geophys. Res.* 104, 20307–20327. doi:10.1029/1999jb900147

Maesano, F. E., Tiberti, M. M., and Basili, R. (2017). The Calabrian Arc: Three-Dimensional Modelling of the Subduction Interface. *Sci. Rep.* 7, 1–15. doi:10.1038/s41598-017-09074-8

Maesano, F. E., Volpi, V., Civile, D., Basili, R., Conti, A., Tiberti, M. M., et al. (2020). Active Extension in a Foreland Trapped between Two Contractional Chains: The South Apulia Fault System (SAFS). *Tectonics* 39. doi:10.1029/2020TC006116

Malinverno, A., Cafiero, M., Ryan, W. B. F., and Cita, M. B. (1981). Distribution of Messinian Sediments and Erosional Surfaces beneath the Tyrrhenian Sea-Geodynamic Implications. *Oceanol. Acta* 4, 489–495.

Malinverno, A., and Ryan, W. B. F. (1986). Extension in the Tyrrhenian Sea and Shortening in the Apennines as Result of Arc Migration Driven by Sinking of the Lithosphere. *Tectonics* 5, 227–245. doi:10.1029/tc005i002p00227

Maramai, A., Graziani, L., and Brizuela, B. (2019). Italian Tsunami Effects Database (ITED): the First Database of Tsunami Effects Observed along the Italian Coasts. *Nat. Hazards Earth Syst. Sci. Discuss.* 9, 1–21. doi:10.5194/nhess-2019-241

Mariucci, M. T., and Montone, P. (2020). Database of Italian Present-Day Stress Indicators, IPSI 1.4. *Sci. Data* 7, 1–11. doi:10.1038/s41597-020-00640-w

Michelini, A., Lomax, A., Nardi, A., and Rossi, A. (2006). "La localizzazione del terremoto della Calabria dell'8 settembre 1905 da dati strumentali," in *8 Settembre 1905, Terremoto in Calabria*. Editors I. Guerra and A. Savaglio (Calabria, Calabria: Università della Calabria), 225–240.

Miller, M. S., Gorbatov, A., and Kennett, B. L. N. (2006). Three-dimensional Visualisation of a Near-vertical Slab Tear beneath the Southern Mariana Arc. *Geochemistry, Geophys. Geosystems* 7. doi:10.1029/2005gc001110

Monaco, C., and Tortorici, L. (2000). Active Faulting in the Calabrian Arc and Eastern Sicily. *J. Geodynamics* 29, 407–424. doi:10.1016/S0264-3707(99)00052-6

Neri, G., Caccamo, D., Cocina, O., and Montalto, A. (1996). Geodynamic Implications of Earthquake Data in the Southern Tyrrhenian Sea. *Tectonophysics* 258, 233–249. doi:10.1016/0040-1951(95)00202-2

Neri, G., Orecchio, B., Totaro, C., Falcone, G., and Presti, D. (2009). Subduction beneath Southern Italy Close the Ending: Results from Seismic Tomography. *Seismological Res. Lett.* 80, 63–70. doi:10.1785/gssrl.80.1.63

Nijholt, N., and Govers, R. (2015). The Role of Passive Margins on the Evolution of Subduction-Transform Edge Propagators (STEPs). *J. Geophys. Res. Solid Earth* 120, 7203–7230. doi:10.1002/2015jb012202

Orecchio, B., Presti, D., Totaro, C., and Neri, G. (2014). What Earthquakes Say Concerning Residual Subduction and STEP Dynamics in the Calabrian Arc Region, South Italy. *Geophys. J. Int.* 199, 1929–1942. doi:10.1093/gji/ggu373

Pepe, F., Bertotti, G., Ferranti, L., Sacchi, M., Collura, A. M., Passaro, S., et al. (2014). Pattern and Rate of post-20 Ka Vertical Tectonic Motion Around the Capo Vaticano Promontory (W Calabria, Italy) Based on Offshore Geomorphological Indicators. *Quat. Int.* 332, 85–98. doi:10.1016/j.quaint.2013.11.012

Pepe, F., Sulli, A., Bertotti, G., and Cella, F. (2010). Architecture and Neogene to Recent Evolution of the Western Calabrian continental Margin: An Upper Plate

Perspective to the Ionian Subduction System, central Mediterranean. *Tectonics* 29, 1–24. doi:10.1029/2009TC002599

Piatanesi, A., and Tinti, S. (2002). Numerical Modelling of the September 8, 1905 Calabrian (Southern Italy) Tsunami. *Geophys. J. Int.* 150, 271–284. doi:10.1046/j.1365-246x.2002.01700.x

Piromallo, C., and Morelli, A. (2003). P Wave Tomography of the Mantle under the Alpine-Mediterranean Area. *J. Geophys. Res. Solid Earth* 108. doi:10.1029/2002jb001757

Polonia, A., Torelli, L., Artoni, A., Carlini, M., Faccenna, C., Ferranti, L., et al. (2016). The Ionian and Alfeo-Etna Fault Zones: New Segments of an Evolving Plate Boundary in the central Mediterranean Sea?. *Tectonophysics* 675, 69–90. doi:10.1016/j.tecto.2016.03.016

Polonia, A., Torelli, L., Mussoni, P., Gasperini, L., Artoni, A., and Klaeschen, D. (2011). The Calabrian Arc Subduction Complex in the Ionian Sea: Regional Architecture, Active Deformation, and Seismic hazard. *Tectonics* 30 (5). doi:10.1029/2010tc002821

Pondrelli, S., Visini, F., Rovida, A., D'Amico, V., Pace, B., and Meletti, C. (2020). Style of Faulting of Expected Earthquakes in Italy as an Input for Seismic hazard Modeling. *Nat. Hazards Earth Syst. Sci.* 20, 3577–3592. doi:10.5194/nhess-20-3577-2020

Presti, D., Billi, A., Orecchio, B., Totaro, C., Faccenna, C., and Neri, G. (2013). Earthquake Focal Mechanisms, Seismogenic Stress, and Seismotectonics of the Calabrian Arc, Italy. *Tectonophysics* 602, 153–175. doi:10.1016/j.tecto.2013.01.030

Presti, D., Neri, G., Orecchio, B., Scolaro, S., and Totaro, C. (2017). The 1905 Calabria, Southern Italy, Earthquake: Hypocenter Location, Causative Process, and Stress Changes Induced in the Area of the 1908 Messina Straits Earthquake. *Bull. Seismol. Soc. Am.* 107, 2613–2623. doi:10.1785/0120170094

Riuscetti, M., and Schick, R. (1975). Earthquakes and Tectonics in Southern Italy. *Boll. Geof. Teor. Appl.* 17, 59–78.

Rizzo, G. B. (1906). *Sulla velocità di propagazione delle onde sismiche nel terremoto della Calabria del giorno 8 settembre 1905. Mem. R. Accad. Sci., Torino, 1905-1906, s. II, Tom. LVII*. Torino: Mem. R. Accad. Sci..

Rosenbaum, G., Gasparon, M., Lucente, F. P., Peccerillo, A., and Miller, M. S. (2008). Kinematics of Slab Tear Faults during Subduction Segmentation and Implications for Italian Magmatism. *Tectonics* 27, a–n. doi:10.1029/2007TC002143

Rovida, A., Locati, M., Camassi, R., Lolli, B., and Gasperini, P. (2020). The Italian Earthquake Catalogue CPTI15. *Bull. Earthquake Eng.* 18 (7), 2953–2984. doi:10.1007/s10518-020-00818-y

Rovida, A. N., Locati, M., Camassi, R. D., Lolli, B., Gasperini, P., and Antonucci, A. (2021). *Catalogo Parametrico dei Terremoti Italiani CPTI15, versione 3.0*. Istituto Nazionale di Geofisica e Vulcanologia (INGV). doi:10.13127/CPTI/CPTI15.3

Sacks, P. E., and Secor, Jr., D. T., Jr (1990). Delamination in Collisional Orogens. *Geol* 18, 999–1002. doi:10.1130/0091-7613(1990)018<0999:dico>2.3.co;2

Sandron, D., Loreto, M. F., Fracassi, U., and Tiberi, L. (2015). Shaking Scenarios from Multiple Source Models Shed Light on the 8 September 1905Mw 7 Calabria Earthquake (Southern Italy). *Bull. Seismological Soc. America* 105, 912–927. doi:10.1785/0120140044

Scarfì, L., Barberi, G., Barreca, G., Cannavò, F., Koulakov, I., and Patanè, D. (2018). Slab Narrowing in the Central Mediterranean: The Calabro-Ionian Subduction Zone as Imaged by High Resolution Seismic Tomography. *Sci. Rep.* 8, 1–12. doi:10.1038/s41598-018-23543-8

Schwanghart, W., and Scherler, D. (2014). Short Communication: TopoToolbox 2 - MATLAB-Based Software for Topographic Analysis and Modeling in Earth Surface Sciences. *Earth Surf. Dynam.* 2, 1–7. doi:10.5194/esurf-2-1-2014

Scrocca, D., Doglioni, C., and Innocenti, F. (2003). Constraints for an Interpretation of the Italian Geodynamics: a Review. *Mem. Descr. Della Cart. Geol. D'italia* 62, 15–46.

Tansi, C., Muto, F., Critelli, S., and Iovine, G. (2007). Neogene-Quaternary Strike-Slip Tectonics in the central Calabrian Arc (Southern Italy). *J. Geodynamics* 43, 393–414. doi:10.1016/j.jog.2006.10.006

Tiberti, M. M., Vannoli, P., Fracassi, U., Burrato, P., Kastelic, V., and Valensise, G. (2017). Understanding Seismogenic Processes in the Southern Calabrian Arc:a Geodynamic Perspective. *Ijg* 136, 365–388. doi:10.3301/IJG.2016.12

Tortorici, L., Monaco, C., Tansi, C., and Cocina, O. (1995). Recent and Active Tectonics in the Calabrian Arc (Southern Italy). *Tectonophysics* 243, 37–55. doi:10.1016/0040-1951(94)00190-K

Totaro, C., Orecchio, B., Presti, D., Scolaro, S., and Neri, G. (2016). Seismogenic Stress Field Estimation in the Calabrian Arc Region (South Italy) from a Bayesian Approach. *Geophys. Res. Lett.* 43, 8960–8969. doi:10.1002/2016GL070107

van Dijk, J., and Okkes, M. (1991). Neogene Tectonostratigraphy and Kinematics of Calabrian Basins; Implications for the Geodynamics of the Central Mediterranean. *Tectonophysics* 196, 23–60. doi:10.1016/0040-1951(91)90288-4

van Dijk, J. P., Bello, M., Brancaleoni, G. P., Cantarella, G., Costa, V., Frixa, A., et al. (2000). A Regional Structural Model for the Northern Sector of the Calabrian Arc (Southern Italy). *Tectonophysics* 324 (4), 267–320. doi:10.1016/S0040-1951(00)00139-6

van Dijk, J. P. (1992). Late Neogene Fore-Arc basin Evolution in the Calabrian Arc (central Mediterranean); Tectonic Sequence Stratigraphy and Dynamic Geohistory. *Faculteit Aardwetenschappen* 25, 26–51. doi:10.1111/j.1365-2117.2012.00549.x

van Dijk, J. P., and Scheepers, P. J. J. (1995). Neotectonic Rotations in the Calabrian Arc; Implications for a Pliocene-Recent Geodynamic Scenario for the Central Mediterranean. *Earth-Science Rev.* 39, 207–246. doi:10.1016/0012-8252(95)00009-7

Williams, G. D., Powell, C. M., and Cooper, M. A. (1989). Geometry and Kinematics of Inversion Tectonics. *Geol. Soc. Lond. Spec. Publications* 44, 3–15. doi:10.1144/gsl.sp.1989.044.01.02

Wortel, M. J. R., and Spakman, W. (2000). Subduction and Slab Detachment in the Mediterranean-Carpathian Region. *Science* 290, 1910–1917. doi:10.1126/science.290.5498.1910

Conflict of Interest: The authors declare that the research was conducted in the absence of any commercial or financial relationships that could be construed as a potential conflict of interest.

The reviewer SB declared a shared affiliation with one of the authors, DC, to the handling editor at time of review.